The Hydrogeology of Curaçao: an electrical resistivity study

Anne Fleur Mineke van Leeuwen

MSc Thesis

Hydrology and Quantitative Water Management Group
Wageningen University, April 2022

Abstract

Worldwide, coral reef health is declining rapidly due to both global stressors (climate change) and local stressors (pollution). Reef maintenance on Curaçao focusses on reducing local stressors including terrestrial pollution. One flow path for terrestrial pollution is via submarine groundwater discharge (SGD). Yet, on the island of Curaçao these hotspots of submarine groundwater discharge have not yet been located, let stand quantified. With this research we aimed to increase our understanding of groundwater flow on the island. This will serve as a foothold for future SGD research. To do so, we have conducted 9 electrical resistivity tomography (ERT) measurements to understand (1) the heterogeneity of the lava formation, the main aquifer, (2) the saltwater-fresh water interface at the coast, and (3) the groundwater flow at geological interfaces. To assist in the interpretation of the data we measured groundwater levels and the discharge of Hato spring, in addition to observing local geological outcrops. We discovered that the lava formation is a very heterogenous aquifer due to variety in degree of weathering of the pillow basalt. As a result of the heterogenous permeability, the extent of seawater intrusion in the coastal lava formation is strongly variable. Yet, the lava formation does form a better barrier for sea-fresh water mixing than the limestone terraces. The midden formation (sedimentary rock) forms a thin aquifer near the surface. And, at the interface of lava and midden formation, the groundwater flow is hampered. As a result, the groundwater is confined within the lava formation until the lava formations reservoir "overflows". The same occurs at the interface of the lava formation and the diorite intrusion. The next step in SGD research is quantifying the seaward groundwater flux where the lava formation is in direct contact with the sea or limestone formation. Here seaward groundwater flow is not hampered by the midden formation or the intrusion and thus forms hotspots of Submarine (polluted) Groundwater Discharge.

Contents

1 Introduction

1.1 Problem description

Local anthropogenic influence has already damaged 60% of the coral reefs worldwide. Combined with rising ocean temperatures, that percentage is expected to rise up to 75% (Burke et al., 2011). Not only are corals "carpets of life" that support a quarter of all marine life (OHI, 2017), but especially on small island development states (SIDs) they also contribute to human welfare. SIDs, such as Curaçao, are highly depended on coral reef ecosystem services. For Curaçao, the reefs form >80% of the coastal protection and a major source of income through tourism (Burke et al., 2011).

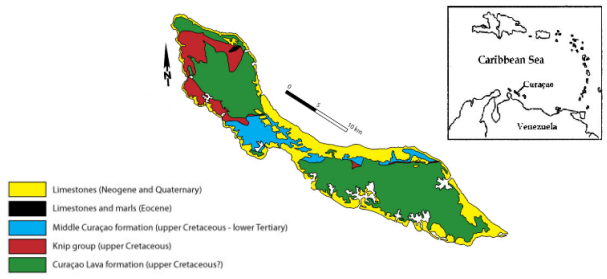

Figure 1: Curaçao: a small island state in the Southern Caribbean Sea.

To save the coral reefs of Curaçao, the causes of coral death need to be identified. One presumed evil is the leaching of (terrestrial) pollutants to sea (WAITT, 2016). Curaçao does not have a proper sewer system in place. The treatment plants are too small and not fully operational. In addition, domestic septic tanks are often poorly maintained and wastewater is illegally dumped. Thus, pollutants can easily leach into the groundwater and are then carried to the sea (Erdogan, 2021).

Once groundwater seeps into the coastal zone, it is also referred to as Submarine Groundwater Discharge (SGD). Recent studies have highlighted the relationship between coral growth and SGD, implying that SGD forms a conduit for pollutants which impact reef processes (Lubarsky et al., 2018). Besides SGD, runoff during high intensity rainfall events can also carry pollutants and sediment to sea. As a result, runoff is a fast and intermittent conduit of pollutants, whereas SGD forms a slow, continuous source of pollution. The study of these processes on Curaçao will be the focus of the SEALINK project (SEALINK, n.d.).

The last large scale attempt at explaining and quantifying the hydrology of Curaçao was done by Abtmeier in the late 1970's (Abtmaier, 1978). Based on his calculations we can assume that the groundwater recharge was equal or smaller than the runoff flux. Yet, since 1962 the authority of Curaçao stopped pumping up water and Shell followed in 1973 (Abtmaier, 1978). And, whilst Abtmaier estimated the groundwater recharge in 1977, some years after commercial pumping was terminated, the groundwater levels may not have been fully restored to equilibrium by then. Because the recharge flux is very small and the precipitation regime inconsistent, see figure 1, the climate of Curaçao is classified as semi-arid. Under these conditions the restoration time of the groundwater table post pumping is increased (Seo et al., 2017). In addition, the recent water-infrastructural changes may have led to new water inputs: irrigation, sewage and leakage of water from the desalinisation plant. These new freshwater fluxes will increase groundwater levels, freshen the aquifer and reduce saltwater intrusion.

The groundwater recharge also depends on the hydraulic properties of the subsurface. Curaçao is made up of multiple geologies, see figure 1. These various formations have experienced phases of folding, faulting, tilting(Kambesis et al., 2016), which impact the groundwater flow. As a result, the hydraulic properties of the subsurface are not only dependent on the underlying rock type, but also by the aforementioned tectonic deformations. On top of that, it is unclear to what extent the groundwater flux is trans-boundary (can cross into other geological formations).

To uncover how groundwater behaves per geology and geological interface, we will mainly use Electrical Resistivity Tomography. This technique will allow us too "see" into the subsurface to (1) distinguish different geologies and characteristics and (2) locate the groundwater table, see section 3.1.1. These observations need to be ground truth-ed with additional information gathered from: local geology field surveys, water level and electrical conductivity measurement's of the groundwater.

Thus, to fully understand the behaviour of groundwater and the effects caused by the changes in water management over the last $\approx$ 50 years, we need to understand the groundwater flow through each geology and geological interface. Then, we can better locate areas with high chances of Submarine Groundwater Discharge. It's time to look under the carpets of life and save the coral reefs.

1.2 Previous research

In the past, there has been thorough research into the hydro(geo)logy of Curaçao. Here we will summarize the geology and relevant hydro(geo)logical findings of the aforementioned Abtmaier and a more recent case study of the groundwater resources of PortoMari by (Morgan et al., 2001) conducted in 2001. The PortoMari case study includes electrical resistivity measurements techniques that were also be applied in this study. This infor-

mation combined form the backbone for understanding the hydro(geo)logy of Curaçao.

1.2.1 Geology of Curaçao

Curaçao has a volcanic origin. In the Cretaceous–Danian age tholeiitic lava and tuffs were excreted predominantly below sea level (Hippolyte & Mann, 2011) (Westermann, 1949). The lavas are at least 1 km thick (Beets, 1972). Klaver (1987) even propesed that the lava formation is a 5 km thick section of submarine basalts, with only pillow basalts at the bottom of the sequence to pillow basalts, hyaloclastites, and sills at the the surface, see figure 2. The variability in thickness described in these two studies reflects the variability in weathering of the lava formation and the lack of continuous outcrops. As as result, the interpretation of the structural and stratigraphic relationships is difficult and increases the uncertainty of the stratigraphics like in figure 2 is. No erosional horizons or sedimentary interbeds have been observed, despite the multiple volcanic pulses (Loewen et al., 2013). In addition, the trace element patterns of the lava formation are uniform(Klaver, 1987) (Kerr et al., 1996). Therefore, the lava formation must represent a continuous or intermittent magma generation from a mantle source over a period of 30 million years (Loewen et al., 2013).

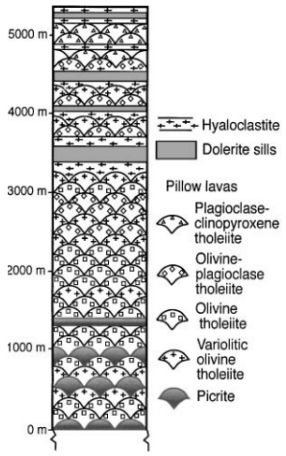

Figure 2: Generalized stratigraphic column of the Curaçao lava formation (after (Klaver, 1987)) taken from (Kerr et al., 1996)

During episodes of higher sea levels in the Upper-Cretaceous sediments were deposited, resulting in the knip formation. The knip formation can mostly be found in the east part of the island and to a lesser extent in the west (Westermann, 1949). In the west, the knip formation is also referred to as the Ronde Klip formation named after the nearby "Landhuis" (Molengraaff, 1929) but we will refer to it as knip formation from now on. The knip formation is maximum 500 m thick and consists out of layers of tuffs, lava breccias, shales, gravels and limestone rubble.

In the upper-Cretaceous light folding of the crust occurred allowing the formation of the Seroe Teintje limestone. Followed by a new episode of sub-marine sedimentation of material: the midden formation. It is believed that the midden formation was more than a thousands meter thick (Westermann, 1949). The midden formation is predominantly found in the center of the island, hence the name, see figure 1. The midden formation has a very clear stratigraphic layering. From top to bottom (e.g. young to old) the midden formation is composed of: (a) 200-550 m thick conglomerates from local eroded material, (b) >700 m thick sandstone and shales, (c) shales of unknown thickness(Westermann, 1949).

Intensive orogeny took place during the Tertiary: the Laramide orogeny. During this period of extensive folding, there was an intrusion of diorite in the north-east of Curaçao. At Ronde Klip, the intrusion caused contact metamorphosis of the surrounding tuffs. It has been suggested that there are more diorite intrusions over the entire island, but that these have never reached the (near)surface (Molengraaff, 1929).

Finally, In the Quaternary, a fringing reef formed 2 to 4 limestone terraces around the entire coast, see figure 1 (van Buurt, 2009). The terraces can roughly be subdivided into a lower and a higher terraces, see figure 3 (Muhs et al., 2012). During the episodes of higher sea levels in the past, caves and blowholes have formed in the limestone terraces that are now no longer below sea level (Kambesis et al., 2016).

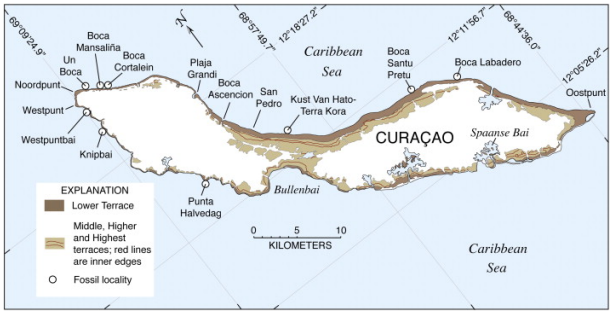

Figure 3: Map of the Lower Terrace and all higher terraces on Curaçao based on (de Buisonjé, 1974), taken from (Muhs et al., 2012).

The older geologies, lava, knip and midden formation have been strongly folded during the various folding phases. As a result, the lava formation has metamorphosed to the zeolite facies. These units are overlain by weakly folded limestones from the Eocene (Kambesis et al., 2016). To this day, we can still observe the main convexes and concaves due to the folding. In the length of

the island, from the north-west to the south-east, there is the main anticline (Kambesis et al., 2016). Whereas in the width, orthogonal to the main anticline, there is an anticline in the east and west, but a syncline in the center of Curaçao (Molengraaff, 1929).

The best geological map available is that of Beets (1977), see appendix figure 1. The map also includes extra information on rooi's and the dip and strikes of geologies. Abtmeier did discover one error in Beets map: the area at Ronde Klip identified as midden formation by Beets (1977) is actually lower limestone terrace covered with chert rubble (Abtmaier, 1978).

1.2.2 Hydro(geo)logy of Curaçao (Abtmaier, 1978)

Abtmaier, as previously mentioned, conducted the last large scale investigation on the groundwater of Curaçao. As the main goal of his research was to estimate groundwater availability, he followed a water balance approach and estimated the groundwater recharge within the watersheds of the island. In addition to doing pumping tests, he measured the water levels and Electrical Conductivity (EC) in $\approx$ 290 wells and boreholes. Together with data on precipitation, spring discharge and hydrochemistry, Abtmaier explained the variation in hydrogeologic properties between the different geologies.

The results of Abtmaiers pumping tests and averaged measured EC values of the groundwater are shown per geology in table 1. The lava formation has the highest transmissivity (kD) which makes it the most important groundwater recharge area of Curaçao. Yet, Abtmaier hints that the high kD of the basalt is due to the weathering at surface. The degree of weathering and the resulting fracturing of the lava formation decreases with depth based on his geological borehole descriptions. The depth of the un-weathered lava formation, i.e. aquifer base, has not been reached in the geological boreholes. Nonetheless we can assume that the the kD decreases with depth.(Abtmaier, 1978).

The EC is generally quite high on the island. This is due to fossil seawater in the formations and sea spray. The fossil seawater is predominantly found in the knip- and midden formation see chapter 1.2.1, whereas sea spray increases the salinity of the surface over the entire island. Abtmaier found that in some cases, pumping has increased the EC by enhancing the saltwater intrusion, especially in the knip- and midden formation. He also hypothesized that salt intrusion, via air or sea, is quickly diluted in the lava formation due to the permeable surface layer and high groundwater recharge. In the limestone saltwater intrusion may be limited due to the presence of impermeable marl layers (Abtmaier, 1978).

Verweerde diabaas kan onder den zeespiegel voorkomen, omdat het eiland minder 118 hoog is opgeheven, dan het voordien beneden den zeespiegel is gedaald. Indien deze putten zeer diep gemaakt worden, zal het opgepompte water brak zijn. (molengraff)

Table 1: The formations of Curaçao and their properties (Abtmaier, 1978)

Formation	kD (m^2/d)	EC ($\mu S/cm$)
Lava Formation	50-200	1250-2250
Knip	5	2500-4000
Midden Formation	5	20000-50000
Limestone	-	above marl: 3000 below marl: 8000 no marl: 20000

The lava formation may be the main aquifer according to Abtmaier, the recharge flux he has computed is still quite low. Due to the semi-arid climate, precipitation regime and land use, the groundwater recharge on the basalt is a mere 4% of precipitation in the SE and 2% in NW of the island. On average that equals to 24 mm and 12 mm a year. These values give a first-based estimate of Submarine Groundwater Discharge (SGD) of Curaçao: assuming a steady state situation, groundwater recharge has to equal the outflow to sea. After all, what goes in must go out. However, it is unclear how these values were computed. In addition he neglected the occurrence of runoff during high intensity rainfall events. He mentioned a paper by Grontnij & Sogreagh in which they computed the runoff to be between 3% and 18% of the yearly rainfall, depending on how "wet" the year was (Grontmij & Sogreah, 1968). Yet, both the Grontnij & Sogreagh and Abtmaier did not trust these results, because the calculations were based on unsuitable empirical observations. To make matters worse, the paper of Grontnij & Sogreagh is no longer available.

Abtmaier also measured the discharge of a number of springs. Table 2 shows the monthly measured discharge (l/s) and the measured EC ($\mu S/cm$) of one of these springs: Hato spring. The other springs will not be discussed here as they are outside our research area and/or have a small discontinuous discharge. Because of the distinct dry period on Curaçao, see chapter **??**, we hypothesize that a spring with a discontinuous discharge must have a small recharge area and/or a small groundwater reservoir. As our focus is on the larger hydrogeological scale processes, these springs will not be taken into account.

Hato spring emerges at the border of the middle terrace (limestone) and the midden formation, where the contact zone is exposed. Table 2 shows the measured discharge (l/s) and the measured EC ($\mu S/cm$). Abtmaier believes the spring is fed by rainwater that seeps through

the limestone until it reaches the midden formation, an aquitard.

1.2.3 Electrical Resistivity Case study: PortoMari Plantage (Morgan et al., 2001)

In 2001, Morgan et al. did an extensive assessment of the groundwater resources at the PortoMari Plantages. PortoMari is located on the Midden-Formation on the north west coast of Curaçao, see figure 4. Their study includes electrical resistivity measurements similar to those used in our research, see chapter 3.1.1. They also used borehole drilling reports to ground truth these measurements. However Morgan et al. are sceptical about the quality of these borehole drillings, because they line up poorly with their electrical resistivity profiles.

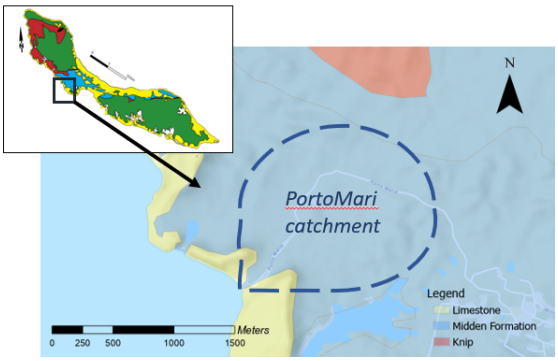

Figure 4: The PortoMari catchment on the north west coast of Curaçao.

Overall this study concluded that: (I) the surface has a high resistivity due to it being dried out, (II) the shallow subsurface (<5m) is layered and alternating between weathered/fractured lava formation mixed with clay/sand/silt strata, (III) shallow clay layers create pseudo groundwater levels and, (IV) from 10 to 25m there is a deeper resistive zone. This deeper resistive zone is below the water table which is odd because in general, saturation of pore space should result in *decreasing* resistivities(Tørå et al., 2010). Morgan et al. (2001) are not clear on the exact composition of the deeper resistive zone. But, they do stress this layer must be highly permeable due to the lack of saline features. The midden formation is a marine sedimentary rock and thus is saline in origin. The salt can only be removed by flushing the subsurface with fresh(ground)water. A salt reduction in in the midden formation via flushing would explains the observed increase in resistivity. Alternatively, Morgan et al. propose that the resistive zone is due to a reduction of water content with depth, possibly there is a subterranean channel or air pocket.

The overall resistivities found in the PortoMari catchment are low, see table 2. Especially compared to Abtmeier, who also did some electrical resistivity measurements and came across higher value for diabase (here Lava Formation). He measured a resistivity of 50-90 $\Omega.m$.(Abtmaier, 1978).

Table 2: The geologies at PortoMari and their depth, measured resistivities: R_a, and changeability: m_a

Geology	depth [m]	R_a [$\Omega.m$]	m_a[%]
(saline) clay	9-15	14	0.8
diabase	6-10	25	0.75
75% limestone sand & clay 25%	10-2	40	1.7

1.3 Research Questions

The main research question is: "How do the hydrological properties of each geological formation impact the groundwater flow through time and space?" To answer the main research questions, we first need to know how the permeability of the formations vary. The Lava Formation forms the main aquifer of the island (Abtmaier, 1978), yet it has been subjected to many deformations (folding, faulting and weathering) which may hamper or form conduits for groundwater flow. It is also unclear if the groundwater flow from the lava formation is hampered at geological interfaces or by salt water intrusion. Fresh water float on seawater and creates a groundwater bulge. The degree of seawater intrusion depends on the penetrability of the coastal formation. Lastly, we need to understand how groundwater levels react to precipitation to get a better spatial and temporal understanding of groundwater flow.

The above unknowns are summarized in the following sub-questions:

- How heterogeneous is the permeability of the Lava Formation?
- To what extent does salt water intrusion occur in the coastal limestone and lava formation?
- How do geological interfaces impact the groundwater flow?
  - What happens at the midden and lava formation interface and how does this link to Hato Spring?
  - What is the influence of the diorite intrusion on groundwater flow?
- How is the temporal and spatial variation of the groundwater levels?

2 Field site description

2.1 Climate

The groundwater recharge on Curaçao is limited due to the climate. Curaçao has a semi-arid climate with a distinguished wet season from September till January (CBS, 2021). On average it rains 70 days a year with the annual precipitation amounting to 600 mm/yr. To put this in perspective, the Netherlands has on average 170 rain days and amounting to 800 mm/yr (Meteo.cw, 2010) (Klimaatinfo, 2021). In addition, Curaçao is subjected to the whims of ENSO. During an El-Niño there are extended periods of drought, whereas in during a La-Niña there is excessive rainfall. Annual precipitation thus fluctuates between 287 mm, El Niño in 2019, to 1092 mm, la Niña 2010, (CBS, 2021). The rain season of 2020-2021, there was a weak La Nina (WMO, 2021)). This means the field campaign occurred in a relatively wet year.

2.2 Measurement locations

2.2.1 Electrical Resistivity Tomography measurements

In order to answer the research questions, we selected The ERT locations based on the following a set of factors.

- geology: to map groundwater in the lava formation, limestone, the lava and midden formation interface and the diorite intrusion.
- proximity to sea: to investigate the extent of seawater intrusion in the lava formation and limestone.
- vicinity of groundwater wells, outcrops and/or geological borehole descriptions of Abtmaier. These are needed to verify/interpret the ERT measurement.
- accessibility: the ERT equipment is heavy ($\pm$ 60 kg) and must be transported by car. In addition, the ERT measurement takes up quite some space (max 155 m) thus a long stretch of cleared land is preferred. Lastly, on private properly permission of the landowner is a necessity.

Based on the aforementioned required factors, we selected 7 ERT locations, see figure 5. We classified these ERT locations based on the reason of interest. This classification structure will be used throughout this research. Table 3 shows an overview of the ERT locations and classifications which will also be discussed below.

Inland Lava Formation Three ERT measurements were performed on inland lava formation: Parallel weg, Centrum Supermarket PSB, and Klein Kwartier. Inland

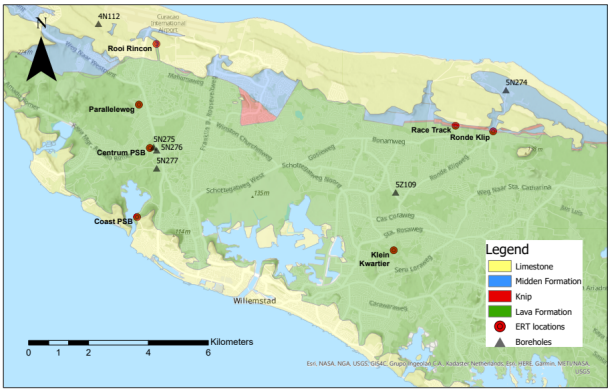

Figure 5: Locations ERT measurements, nearby boreholes described by (Abtmaier, 1978) and the geology

meaning the ERT loactions were not on the coastline. The ERT at Parallel weg next to the groundwater well with the longest timeseries: GW029, see chapter 3.2. The ERT measurement was performed alongside the public road Parallel weg, hence the name. In this area, the locals mentioned a large spatial variability in groundwater levels within their neighbourhood. Some wells would be dry, whilst others would continuously provide water.

Centrum Supermarket PSB is located $\approx$ 1.5 km south of Parallel weg, yet differs from topography as it's situated in a rooi. A rooi is a drainage channel for excess rainfall, which means there is probably a thick alluvium layer at this ERT location. This location is situated next to a well, and two geological borehole drillings: 5N275 and 5N276.

Unlike Paralle weg and Centrum Supermarket PSB, the third location, Klein Kwartier, is located east of Willemstad. Klein Kwartier is currently managed by the government who use the area to infiltrate treated wastewater. The treated wastewater is led through a serie of infiltration ponds and so forms a additional groundwater recharge flux. At Klein Kwartier there was no mention of spatial heterogeneity in groundwater level as observed at Parallel weg. Instead, the government officials praised the quality [1] and continuous availability of water. This makes sense as the area receives extra water from the sewage plant. G.H.J. Molengraaf (1929) has mentioned that the diabase of this area is not thoroughly weathered, resulting in a lower permeability compared to other areas with lava formation. In line with Molengraafs (1929) observation, locals have also mentioned that this area is prone to flooding. After all, a low permeability leads to a low storage capacity of infiltrated rainwater and increased risk of surface runoff.

[1] We have found that on Curaçao locals determine the quality of groundwater based on salinty and oil pollution only.

Coastal ERT Transects Two measurements were done on the coastline. One on the limestone terrace at San Nicolas and one on the Lava formation along the inlet of Piscadera Bay. The limestone terrace at San Nicolas was the only ERT measurement that we did on the west side of the island. Here there was enough space for the measurement, it was easily accessible by car and there is a limestone outcrop. The GWL of the nearby well however could not be measured. The ERT at Piscadera Bay site is an abandoned construction site. The initial slope has partially been removed to create a flattened terrace. As a result, barely any soil remained. The site was next to a nearby lava outcrop in addition to a groundwater well.

Geological Interfaces It is one thing to predict groundwater characteristics in uniform geologies, but another to understand the influence of geological interfaces on groundwater flow. We did 3 ERT measurements on non-uniform geologies: Rooi Rincon, Ronde Klip and the Race track. At Rooi Rincon we measured in the abrasion gully. Here the overlaying limestone has eroded away, exposing the interface between the lava formation and the midden formation (Molengraaff, 1929) (Beets, 1977). Inland of the Rooi Rincon ERT measurement location, there is monitoring well and towards the coast there is Hato spring of which we measured the discharge, see section 2.2.3.

The other two ERT measurements were at the diorite intrusion: Ronde Klip and Racetrack. At Ronde Klip the ERT measurement crosses the lava formation, the diorite intrusion followed by midden formation (Beets, 1977). At Ronde Klip we heard that dynamite was required to remove part of the diorite intrusion, indicating that the diorite rock is still un-weathered. The midden formation here, is actually is actually the lower limestone terrace covered with *alluvial* chert rubble (Abtmaier, 1978). In line with this observation, the current caretaker of the area explained that the area functions as a Rooi and discharges a lot of runoff during (extreme) rainfall events. This runoff contains a lot of sediments which are then deposited on the lower limestone terrace. Despite the presence of the Rooi (which is a input of fresh water) the caretaker complains about brackish groundwater. What is even more odd is that Ronde Klip plantations were previously known for having plenty of good quality water. Due to the lower permeability of the midden and knip formation compared to the lava formation, the groundwater flow is hampered at the geological interface (Molengraaff, 1929). Apparently, this resulted in fresh water conditions in the past, but not in the present. This discrepancy makes this research location even more interesting.

The other ERT measurement on the diorite intrusion, Race Track, is located on the thickest part of the diorite intrusion; $\approx$ 100 m (Beets et al., 1977). Here we also found diorite boulders at the surface. The diorite rock was very hard and very little to no weathering had occurred. Similar to Ronde Klip, a nearby farmer complained about brackish groundwater. He explained that the area along the intrusion is called the "salt highway" in Papiamentu.

2.2.2 Groundwater measurements and monitoring

In order to understand the hydrogeology of Curaçao and assist with the interpretation of the ERT measurements, we did 68 *singular* groundwater level (GWL) and Electrical Conductivity (EC) measurements. In addition we continuously monitored the GWL in 9 other wells on the island. There are two types of wells on Curaçao: hand dug wells and boreholes. Hand dug wells stem from the colonial times. They are wide with diameters of $>$2 m. Generally, the well sides are strengthed with cement till hard rock is encountered at $\approx$ 3 m depth. Hand dug wells are quite shallow with an average of 12 m depth below the surface. Boreholes on the other hand, have an average depth of 27 m below the surface. They are constructed using perforated PVC or metal pipes with a diameter of $\pm$ 25 cm.

Singular Groundwater measurements In collaboration with M. Wit, I. Verstappen and T. Kruijssen, we visited 68 wells and boreholes around the island. For the singular measurements the goal was to get the highest possible spatial variability. Figure 6 depicts all the wells in which the GWL was measured once.

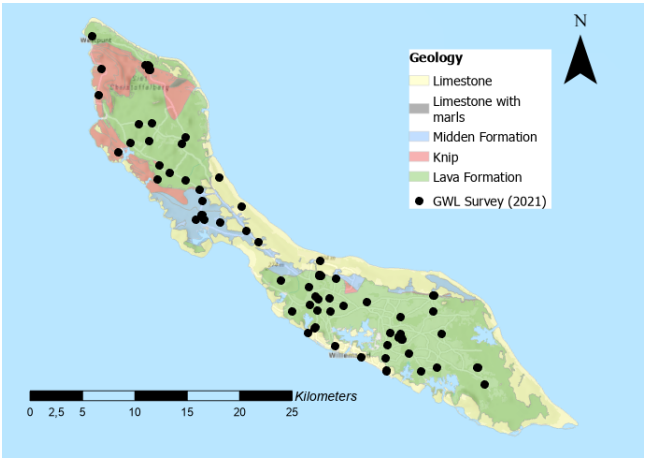

Figure 6: The locations of the singular GWL measurements: GWL survey (2021)

Groundwater Monitoring Sites We monitored the water levels of multiple wells along the island. For this we have striven to create transects crossing the island from north to south, see figure 7. In that way, we could in-

Table 3: An overview of the ERT measurement sites and their specifications

Reason of interest	Site	Geology	notes
Inland lava formation	Parallelweg	Lava Formation	Located next to main groundwater monitoring site: GW029 Garden
	Centrum Supermarket PSB	Lava Formation	Rooi
	Klein Kwartier	Lava Formation	Next to 2 well-monitoring sites and infiltration ponds of (treated) sewage water
Coastal transect	San Nicolas	Limestone	located on the north east coast
	Coast PSB	Lava Formation	Parallel to the inlet of PSB
Geological Interfaces	Rooi Rincon	Lava and Midden Formation	Near Hato spring
	Ronde Klip	Lava Formation and Diorite intrusion	Next to well-monitoring site
	Race track	Lava Formation and Diorite intrusion	-

cludes the topographical water divide which follows the major anticline, see section 1.2.1.

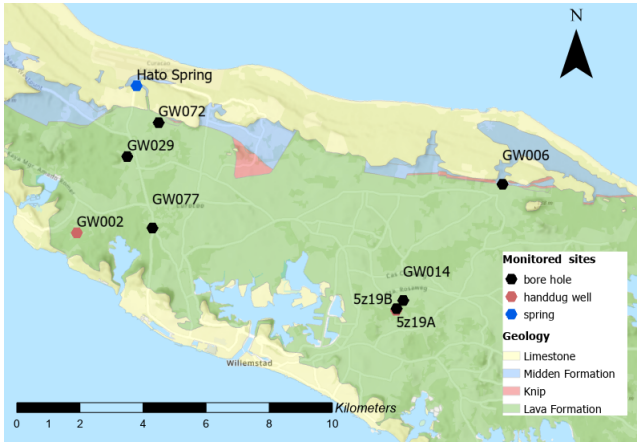

Figure 7: Locations of the 9 monitored groundwater wells: both hand dug (brown) and bore holes (black). In additon to Hato spring (blue) and the geology

2.2.3 Hato spring

The discharge of Hato Spring has previously been measured by Abtmaier, see figure 2 in the Appendix. The discharge is continuous all year-round. Hato spring is located at the interface of limestone and the midden formation. This area is now a nature reserve: Rooi Rincon.

3 Methodology

In order to answer the research questions, we applied electrical resistivity tomography measurements, geological surveys, groundwater and spring measurements. Combined this information will allow us to investigate, interpret and understand the geology and hydrology of the system. As the ERT is the main focus of this study, we will first elaborate on applied electrical resistivity tomography (ERT) technique. The additional information gathered on the geology and (ground)water is predominantly used to better understand and support the conclusions from the ERT results.

3.1 ERT

3.1.1 Background Information

Electrical Resistivity Tomography (ERT) is a widely accepted method to investigate the (hydro)geology of the subsurface. It is based on the principle that subsurface features have different electrical resistivities, see figure 8.

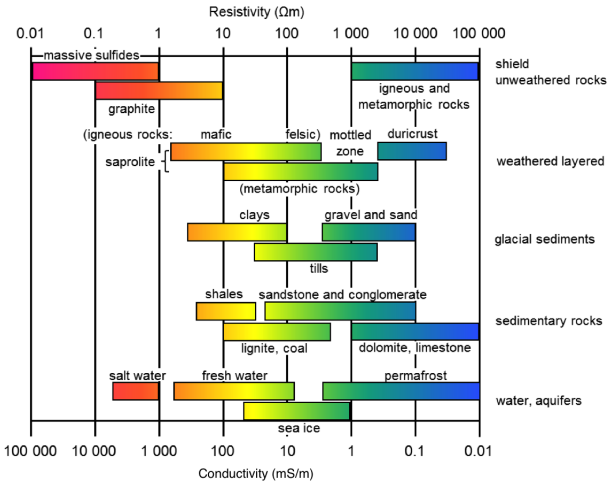

Figure 8: An overview of the resistivities of sediments and rocks (Developers, n.d.)

Resistivity is determined from Ohm's law using the potential difference (voltage) between two electrodes for a known current. At small spacing between electrodes, apparent

The ERT is designed to induce an electrical current into the ground and measure the potential difference (voltage) between the induced and received current. Using Ohm's law the potential difference is converted to the *apparent* resistivity (ρ_a). In our set-up, two electrodes send an electrical pulse into the ground and two receiving electrodes measure the responding current. When multiple electrodes are installed in a row, the user can choose which electrodes will act as sender and receiver. The variety in combinations, called arrays, will determine the type of resolution and investigation depth of the ERT measurement. The latter is also influenced by the spacing between the electrodes. The wider the spacing the deeper electrical pulse can penetrate the subsurface, yet the the lower the resolution will be. In our study, we only used the Wenner-Schlumberger (WS) array and the Dipole-Dipole array (DD). The former is very useful for identifying vertical changes, whilst DD allows for deeper investigation of the subsurface, see figure 9. $C1$ and $C2$ are the current electrodes and $P1$ and $P2$ the receiver electrodes. a is the dipole length and n is the separation factor. k is the geometry factor needed to for the inversion model(Loke, 2004).

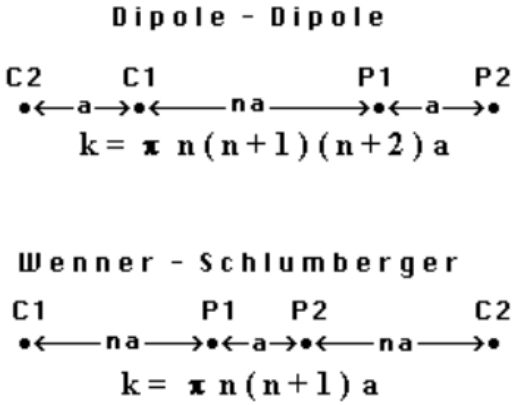

Figure 9: The two arrays used in this research: Dipole-Dipole and Wenner-Schlumberger (Loke, 2004)

As previously mentioned the raw data is referred to as the *apparent* resistivity (ρ_a). In order to interpret the data, the apparent resistivity has to be corrected for the deformation caused by the electrode spacing. For this, an inversion model is used. The inversion model applies a correction factor (the *geometric* factor) to invert the apparent resistivity (ρ_a) to intrinsic resistivity (ρ_i) from which eventually different geological structures can be identified.

However, the interpretation of these inversions is a little less straight forward. As Morgan et al. (2001) previously stated: "Resistivity inversion is as much art and intuition as it is physics and mathematics". To limit the seemingly endless interpretation possibilities, additional measurements can be done with the ERT to increase the quality and understanding of the inversion. A way to distinguish between water and clay, which have similar resistivities, is to measure the changeability of the subsurface. This is done via Induced Polarization (IP). After the ERT has send an electrical pulse into the ground, it does an additional measurement in which it determines

the changeability of the subsurface . Similar to batteries, highly chargeable matrix's, such as clay, can hold electricity for a extended period of time, whereas water cannot. One important side note is that IP measurements do require extra measurement time.

Alternatively or in addition to, one can look to forward modelling. For forward modelling, one conjures up a conceptual model of the subsurface geology and the respective resistivies. The perks of this model being the absence of noise and measurement errors. The forward model is then compared to the inversion to be able to assit in interpretation, see figure (?, ?).

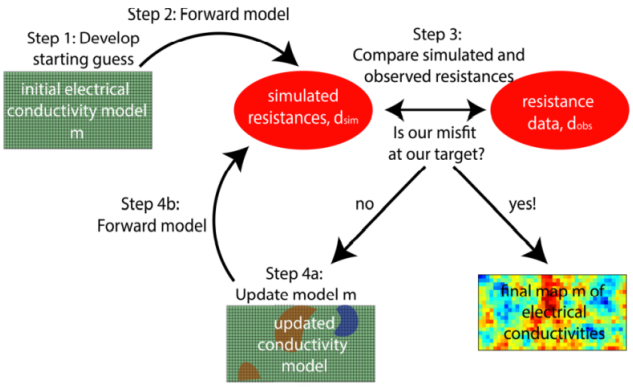

Figure 10: An overview of the inversion taken from: (Johnson et al., 2020)

For the conceptual model, the expected geology can be inferred from field observations and literature, whereas the linked resistivities are computed with the 2 empirical laws of Archie. His 1st law computes the resistivity of fully saturated rock or sediment: R_o, whereas his second law corrects the R_o for unsaturated conditions (G. Archie, 1942). R_o depends on the resistivity of the groundwater: R_w (Ω), the porosity of the material: Φ (-), and the cementation factor m (-), see equation 1. The cementation factor, m, ranges from 1 to 5. The higher the value the less the pores of the substrate are connected. Generally m is set to 2 (Glover, 2009).

$$R_o = R_w \cdot \Phi^{-m} \tag{1}$$

To compute the expected resistivities of unsaturated rocks and sediments, we apply the second law of Archie. The resulting unsaturated bulk resistivity is referred to as R_t (Ω). It is depend on R_o, the water saturation: S_w, and water saturation component: n. Similar to m, n is generally set to 2, but can vary between 1.8 and 4. Lower values are used for matrix's with a lot of clay or fractures, as found on Curaçao.(Glover, 2015)

$$R_t = R_w \cdot \Phi^{-m} \cdot S_w^{-n} \tag{2}$$

The forward modelling approached here will be further discussed in section 3.1.3.

3.1.2 Measurement set-up and Data Collection

The ERT-measurements were performed with the Syscal Pro Switch. Generally, the Syscal Pro switch can host 6 cables with 16 pins each (96 pins in total). The maximum spacing of this set-up is 5m. We had only two cables at our disposal, meaning we had a total of 32 pins covering max 155 m. Because we were mostly interested in the deeper geology, we decided to use the largest spacing possible at each site (5 m). Only at Centrum Supermarket Piscadera bay and at Race Track, space was limited and the spacing was 2 and 4 m respectivly.

The sequences (electrode array & spacing) were made in using Electre Pro and uploaded to the Syscal Pro switch prior to the measurement. In our study, we only used the Wenner- Schlumberger (WS) array and the Dipole-Dipole array (DD). Once the electrodes were installed we performed a resistivity check (R_s). This is a test to identify incorrectly placed electrodes. We strove to get the smallest R_s possible, with 2000 Ω. being the upper limit. Electrodes with a higher resistivity were either reinstalled or, if this was insufficient, we supplied the pin with water and/or mounds of dirt around to increase the connectivity of the pin to the ground. This way, we managed to reduce all electrode resistivities below 2000 Ω.

Figure 11: Land surveying at Piscadera bay. The surveyor looks through the optical level and notes down the height observed of the measuring stick.

During the measurements, we wrote down the GPS location of every electrode and the Syscal Pro Box itself using a Garmin Edge 830. In addition, we used a land surveyor to map the topography of the ERT-transect, see figure 11. The DEM of Curaçao has a too low resolution (5m) for it to be useful in inversion and processing phase of the ERT data.

3.1.3 Data Processing and Interpretation

To extract the data from the Syscal switch pro we used Electre Pro software. Then we imported the apparent resistivity data into ResIPy. ResIPy has advantage that it's an open-source inversion software and rather straight forward to use (Blanchy et al., 2020). For the inversion we used a triangular mesh and checked DOI in the inversion settings tab. The DOI stands for the Depth of Investigation and estimates the depth at which the inversion results have a higher uncertainty. The other inversions settings were kept as standard unless the program indicated that the weights, a_{wgt} and b_{wgt}, were too high. In that case, we decreased the weights 10 fold. After inversion, we checked if most normalized inversion errors were between -3 and 3%. If not, the data was filtered, and the inversion repeated. Repetition of the inversion after post processing does result in the loss of the DOI result.

To assist in interpretation we gathered data from multiple sources:

1. The geology map of Curaçao (Beets, 1977) indicates the surfacing geology.
2. borehole descriptions (Abtmaier, 1978)
3. Local outcrops added additional insights about the soil depth and (deeper) geology.
4. The depth of the groundwater table via wells, in addition to measuring the EC, for methodology see 3.2.

The above information was also used to compute Archies law, see eq 1 and 2. The computed resistivities were used to create conceptual models needed for forward modelling. We only applied them at the ERT transects at geological interfaces. The EC of the ground water (mS/cm) was converted to R_w ($\Omega.m$) as follows:

$$R_w = 1000EC \tag{3}$$

The other parameters to compute the laws of Archie, see eq. 2 and eq. 1, were based on the following: ϕ was based on geological field observations and literature (Qi et al., 2021)(Kambesis et al., 2016). m and n, were estimated using the table from (G. E. Archie, 1952). As the infiltration capacity of the soil is very high and rain events sparse, the soil moisture content must be low. In a LISEM-model study done in Curaçao, the soil moisture content was set to 0.01 (Castrechini Rodriguez, 2021).Table 4 summarizes the used parameters per geology, note R_w is missing this depends on EC of the groundwater measured in the field, see eq. 3.

Table 4: The parameters required to compute the expected resistivity according to Archie's laws.

Geology	n	ϕ	m	S_w
limestone	2	0.5	2.5	0.01
midden-formation	1.8	0.1	1.8	0.01
lava-formation	1.8	0.1	1.4	0.01
diorite	2	0.02	2	0.01

3.2 Groundwater measurements and monitoring

3.2.1 Measurement set-up

Different approaches were used to measure the groundwater level and EC. In line with Abtmeiers approach, me and my colleagues: Titus Kruijssen, Iris Verstappen and Mike de Wit, visited 106 wells and boreholes around the island. There, we measured the groundwater level, did in situ water quality measurements and took water samples. Of these additional measurements only EC and water levels will be used in this research. However, once fully analysed their data will be in a valuable contribution to the understanding of the hydrogeo(chemical) system.

In addition to these singular measurements, we installed micro-divers in order to log the groundwater level over time. The micro-divers measured temperature and the pressure exerted by the water and air columns. Therefore, the measured data has to be corrected for the barometric pressure. For this reason, we installed one barometric pressure sensor in GW029 well. In some cases, we installed a CTD diver instead of/in addition to a pressure sensor diver. The CTD diver measure and logs the conductivity of the water in addition to the temperature and the exerted pressure. Both diver types were set to measure & log the data at least every 30 min. The measurement period differed per location, see table 5. The locations of the monitoring sites follow the same transect approach: orthogonal to the supposed groundwater divide based on the DEM.

At every monitoring sites, we also created EC depth profiles. We did this either with a CTD or manually with a Heron Dipper. In this case we wrote down the EC every 5m and decreased the step size to 1m when we observed a change in EC.

3.2.2 Groundwater data processing

For the singular groundwater levels, the measurements were recorded relative to the surface. In arcGIS Pro, the groundwater measurements were related to the DEM

Table 5: monitoring wells: timestamp, measuring interval and gps coordinates

name	type of well	start measurement	end measurement	interval (min)	diver type	lat	long
Mark	borehole	04/10/2021	04/01/2022	30	micro-diver	-68.9675	12.16233
GW072	borehole	09/11/2021	27/11/2021	30	micro-diver	-68.9585	12.17197
GW002	handdug well	04/11/2021	16/11/2021	30	micro-diver	-68.9819	12.14063
5z19A	handdug well	02/12/2021	14/12/2021	30	CTD	-68.8909	12.11859
5z19B	borehole	02/12/2021	14/12/2021	30	CTD	-68.8907	12.11908
GW014	borehole	23/11/2021	22/12/2021	30	micro-diver	-68.8888	12.12139
GW077	borehole	01/12/2021	03/12/2021	15	CTD	-68.9603	12.14201
Ronde Klip	borehole	12/11/2021	16/12/2021	15	micro-diver	-68.8605	12.15447

to compute the groundwater levels relative to sea level. Then using the kriging method, both the groundwater levels relative to the surface and to sea level were interpolated to a groundwater map for the entire island. The former indicated the general groundwater flow, whereas the latter indicates the general size and location of the freshwater bulge.

The continuous measurements however needed to be corrected by (1) the barometric pressure and (2) the diver depth of the measurement. To better understand the variability of water level in and between other boreholes/wells, the monitored water levels were normalized (NGWL). To do so, the pressure corrected groundwater levels were divided by the initial groundwater level of the respective well. Visual interpretation (trends) of the SGWL along with general statistics (average, standard deviation) and local processes (pumpings ect), indicate the variability and similarity of the groundwater wells. To assist in the interpretation of the trends we will use the weekly precipitation data of Hato airport (Meteo.cw, 2010). NOTE: the rain data only includes the weekly maximum and sum. Therefore we only know when when and how large the maximum rain event was. For the other days, we averaged the precipitation sum (excluding the peak).

3.3 Hato-spring measurements

Hato spring is one of the few continuously flowing springs on Curaçao. At Hato springs we did multiple measurements and applied salt-dilution method to estimate the discharge. The salt-dilution method allows the gauging of streams that are unfit for other measurement techniques (e.g. current meters). The salt dilution method described here is best applied to streams with a small wetted width: $<$2 m , and low flow conditions: $<$100 l/s. The idea is to inject a known salt solution with a constant rate. Then, you can compare the measured EC in the stream with EC and outflow rate of the salt solution using a balance approach.

3.3.1 Measurement set-up

The measurement set-up was a created by a series of trial and error. We used different sized dispensers that were all converted into marionette bottles. The advantage of marionette bottles is that they have a constant discharge. Prior to every experiment, we measured the discharge rate (q) of the marionette bottles.

Then the marionette bottles were filled with a salt solution of a known EC. We want to create a salt solution strong enough to create a measurable increase the in EC, whilst not harming the ecosystem. The required salt concentration (C_{is}) depends on the "allowed" increase in EC (ΔEC) in $\mu S/cm$, the ratio between the estimated discharge of the stream (Q_{est}) and the marionette bottle (q) both in l/s and B (Moore, n.d.). B is a proportionality factor which equals 2.1 (mS/cm)/(g/L) at 25°C, but varies with temperature. (Hongve, 1987)

$$C_{is} = Q_{est}q \cdot \Delta ECB \tag{4}$$

Note that the above equation only holds if spring water is used to make the salt-solution. One can also premix the solution with tap water. For Curaçao, C_{is} will be higher due to the lower EC ($\mu S/cm$) of the tap water (EC_{tap}) compared to that of the stream (EC_{bg}). The equation will then become:

$$C_{is} = Q_{est}q \cdot \Delta EC + EC_{tap} - EC_{bg}B \tag{5}$$

Once the salt-solution is made, we placed two CTD divers in the stream. The first CTD diver was located 5.6 m and another at 15.6 m downstream of the marionette bottle. It is important that the second diver is located beyond the mixing length. A rough guideline is 25 times the width of the stream (Moore, n.d.). In addition we placed a dipper at 14.6 m distance to follow the increase in salinity in real time. The divers were set to at 1 sec intervals. Once all was set, the experiment can be started. We continued the experiment until the EC had stabilized according to the dipper.

3.3.2 Data processing

With this set-up we could both measure the velocity and the discharge of Hato spring. By plotting the CTD results, we can visually determine the required parameters:

Dilution discharge method (Q_{dil}): This is the method for which the salt dilution experiment originally was designed. But in order to compute the discharge, it is important to create a calibration line between the measured EC_{ss} and the Relative Concentration RC. To do so, add salt solution in steps of 5 ml (v_{salt}) of to 250 ml of stream water. At every step measure the EC EC_{cal} in $\mu S/cm$. Continue adding the salt solution 2 to 3 times after the exceeding the measured EC_{ss}. Compute the RC at each step by dividing the total salt solution added by the total volume. Plot the measured EC against the RC and add a trend line going through the origin. The trend should be linear. The directional coefficient of the trend line k. Alternatively, one can compute k as follows:

$$k = \Sigma v_{salt} \cdot (EC_{cal} - EC_{bg})(\Sigma v_{salt} + 250) \quad (6)$$

From the plotted results of $diver2$, the EC of the flattened part of the curve is the EC_{ss}. From the diver data we can also determine the background EC (EC_{bg}) of the spring, in case it was forgotten in the field. The discharge of the spring (Q_{dil}) in l/s can be computed as follows:

$$Q_{dil} = q(k \cdot (EC_{ss} - EC_{bg})) \quad (7)$$

Velocity method (v):
The velocity of the spring can be determined by the time difference between the peaks of EC of the two divers, δ_t (s). For $diver1$, $peak1$ is apparent from the plot. For $diver2$ further downstream, $peak2$ is when the $ECss$ is first reached. In other words when the curve starts to flatten. Then compute velocity, v (m/s), by dividing distance, d (m), by δ_t.

$$\delta_t = t_{peak2} - t_{peak1} \quad (8)$$

$$v = d\delta_t \quad (9)$$

As a check, we also computed the discharge of the stream with computed velocity v. The "wet area", A (dm^2) was estimated by multiplying the water height, h (dm), by the width of the stream, w (dm). With this you can compute the discharge; Q_{velo} (l/s). This is rather inaccurate for the water height will change over time and should be measured again every time a measurement is done. However, we did it once as this is just a verification measurement.

$$A = h * w \quad (10)$$

$$Q_{velo} = A * v * 10 \quad (11)$$

4 Results

Below we will first discuss the results from ERT measurements per class, starting with a description of the geology seen in the field, followed by the ERT inversions and the forward models. Of the latter only those of Rooi Rincon and Race Track will be presented, as the other forward models did not result in any interesting features/discussion points. Some of the DD inversions had very high errors and required post-process filtering. These initial errors are shown in the appendix figures 3 till 7. Lastly, will present the results based on the singular groundwater and measurements monitored groundwater time series.

4.1 Inland Lava Formation:

4.1.1 Local Geology

Based on outcrops near Parallel weg and Centrum Supermarket, the lava formation consists of pillow basalts. The basalt pillows have hard, unfractured, cores, yet the rims of the "pillows" are more fractured, see figure 12 III. This makes the rims more porous and more accessible for roots to penetrate. Also, there are clear signs that these rims are preferential flow paths. We observed calcite precipitation in the rims, see figure 12 I and II. The calcite probably originates from overlaying limestone that has now been fully eroded away.

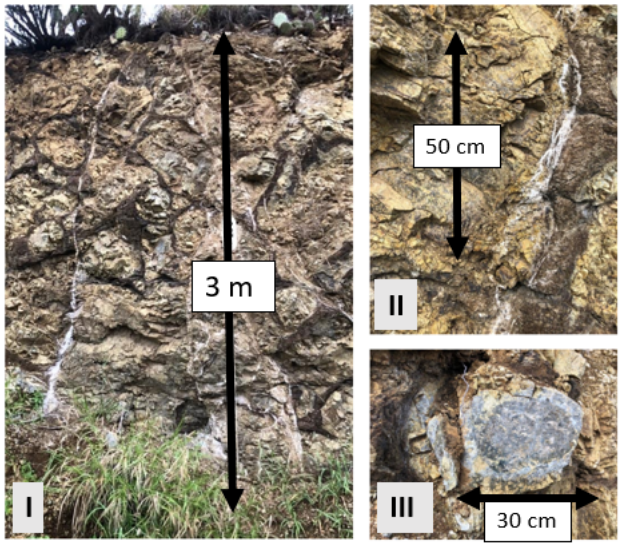

Figure 12: **I** Pillow lava outcrop near Centrum Supermarket PSB, **II** zoomed in on the calcite precipitation and **III** a unfractured pillow basalt core (GPS: 12.141471, -68.955644).

The weathering of the pillow basalt gradually decreases with depth. As a result, the porosity decreases with depth as well. From a hydrological point of view, this means a decrease in water content, even at full saturation. At a certain depth the basalt will be impenetrable for water and act as an aquitard. The base was not observed in the field, but according to borehole descriptions, the basalt is only slightly fractured at 26m depth onward, see appendix figure 2.

4.1.2 ERT: Parallel weg *lava formation*

Here a well was continuously monitored (GW029) and the groundwater level was on average at at 14m depth, see table 6. The measured resistivities are between 2 and 75 $\Omega.m$ for the Dipole-Dipole measurement, and 2 and 312 $\Omega.m$ for the Wenner Schlumberger measurement, see figure 13. Both the inversions were initially very patchy, however the DD inversion had many errors and post process filtering resulted in the smooth picture seen in figure 13 I. The WS data was of better quality and still shows a highly heterogeneous subsurface with very sharp boundaries. There are small patches with high resistivity at above the groundwater level ($<$10 m) and two larger patches below the GWL. Because of the filtering, only one large patch of resistivity in the DD inversion: below the water table at 40 m distance. It must be mentioned that the DOI (dept of investigation) equals the GWL. Thus, the results of the saturated zone are less accurate than at $\leq$ 10 m.

4.1.3 ERT: Centrum Supermarket Piscadera Bay *lava formation*

This location is situated in a rooi south of the Paralelle weg. The groundwater level was measured at 3.5 to 3.8 m depth. Note: The electrode spacing is 2m instead of the 5m at Paralelle Weg and Klein Kwartier. As a result, the resolution is higher, but the penetration depth is shallower.

In figure 14 I & II we can see an increase of resistivity with depth. This is especially visible in the DD inversion, where at from 0 to 45 m distance 7.5 to 10 m depth, there is a uniform area of high resistivity: a bank. This bank stops quite suddenly at 50 m distance. However, the corners of the inversions lie outside the sight of the actual measurement and are extrapolation made by the model. Therefore, it is likely the bank of high resistivity in reality continues further north. The bank is deeper than the DOI of the DD ($\approx$ 3m depth) and this would makes the existence of the bank questionable, if the depth of the bank had not corresponded with a change in lithology in the borehole description, see appendix figure 2. In southern borehole 5N276 at 6 m depth there is a transition from "clay and weathered basalt" to "clay with highly fractured basalt". This decrease in weathered basalt explains the observed increase in resistivity. Whats more, according to

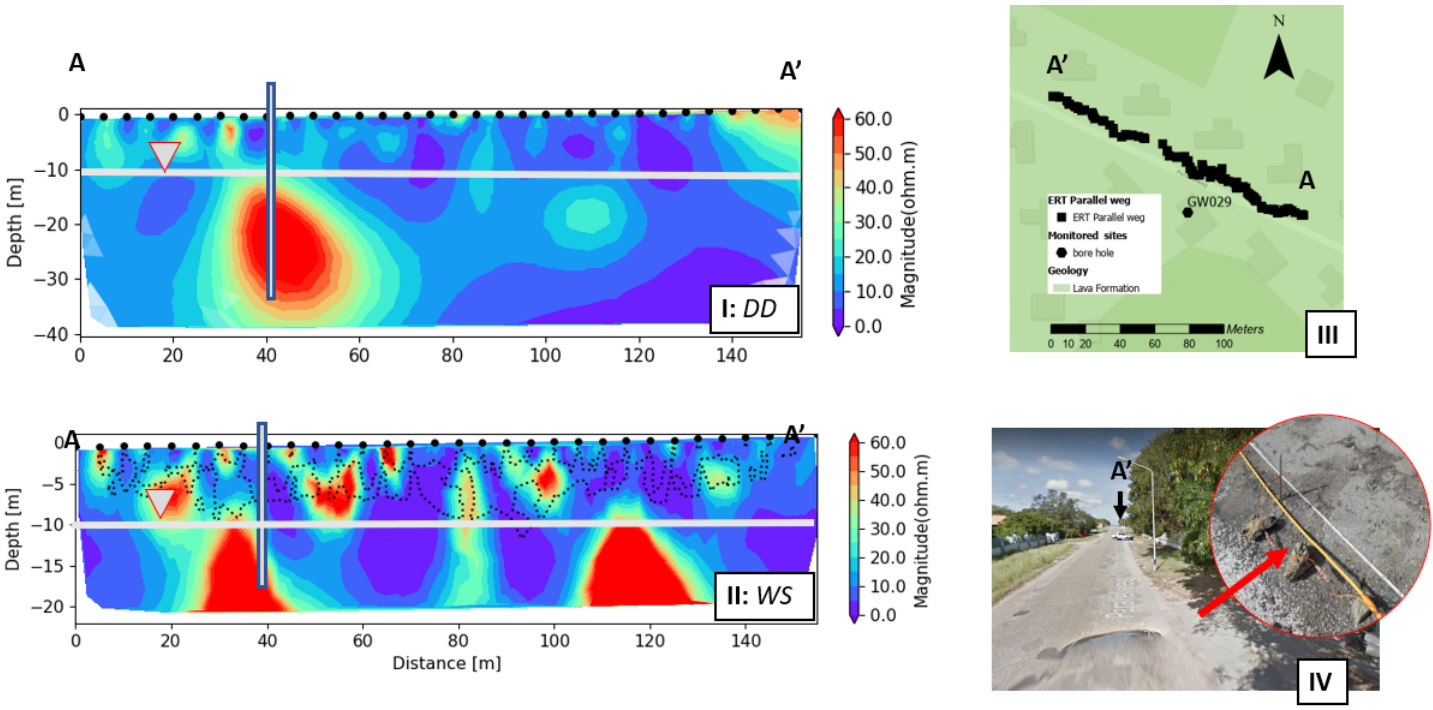

Figure 13: The inversion alongside Parallel weg. **I** is the Dipole-Dipole inversion. **II** below is the Wenner-Schlumberger inversion. **III** shows the local geology, ERT location and monitoring well. **IV** The ERT was layed out along the right side of the road.

borehole 5N275, the depth of the highly fractured basalt increases to 10 m in the north, similar to the increase in depth of the bank in the DD inversion. In addition, the northern borehole 5N275 has includes a layer of basalt with coarse sand, that is absent in 5N276. This explains the light green area in the DD ($\approx$ 45 $\Omega.m$) at 30 to 60 m distance above the bank which is absent more to the south. The DOI of the WS inversion is below the the maximum penetration depth (8m). The WS also shows an increase of resistivity with depth and the effect of the basalt with sand layer is evident, yet the resistive bank is too deep too be seen in the WS inversion.

4.1.4 ERT: Klein Kwartier *lava formation*

The ERT measurement was done parallel to the shore of the last infiltration pond. In the transect there are two wells: 5Z19A and 5Z19B. The former was being pumped during the ERT measurement. The average GWL is 3 m below the surface, see figure 15 III and IV. The resistivity increases with depth. Yet the gradient differs laterally. There are two hot spots of resistivity at 20 m deep at 40 & 110 m distance. Well 5Z19A is located in between these pillars of higher resistivity. The thoroughly weathered layer of the basalt formation is 10 to 15 m thick, see figure 15 I & II.

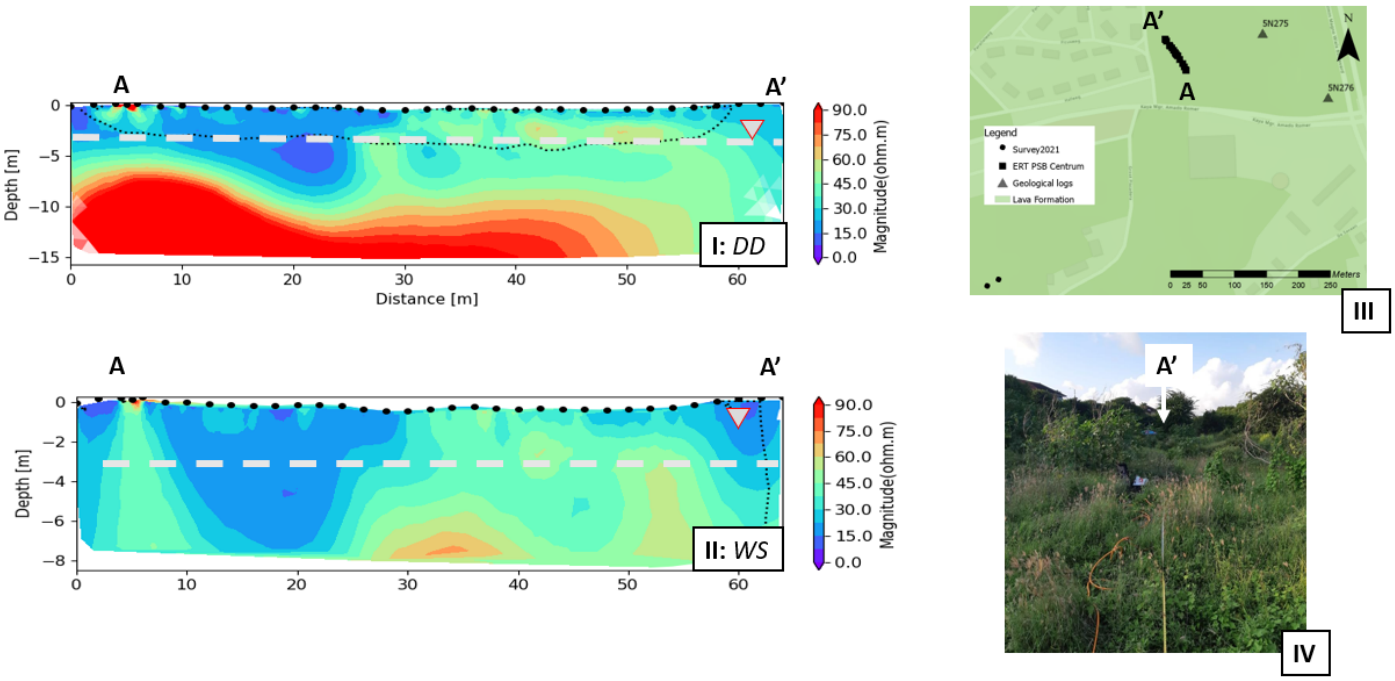

Figure 14: The inversion near the Centrum Supermarket in Piscadera. **I** is the Dipole-Dipole inversion. **II** below is the Wenner-Schlumberger inversion. **III** shows the local geology, ERT location and boreholes. **IV** an impression of the measurement site

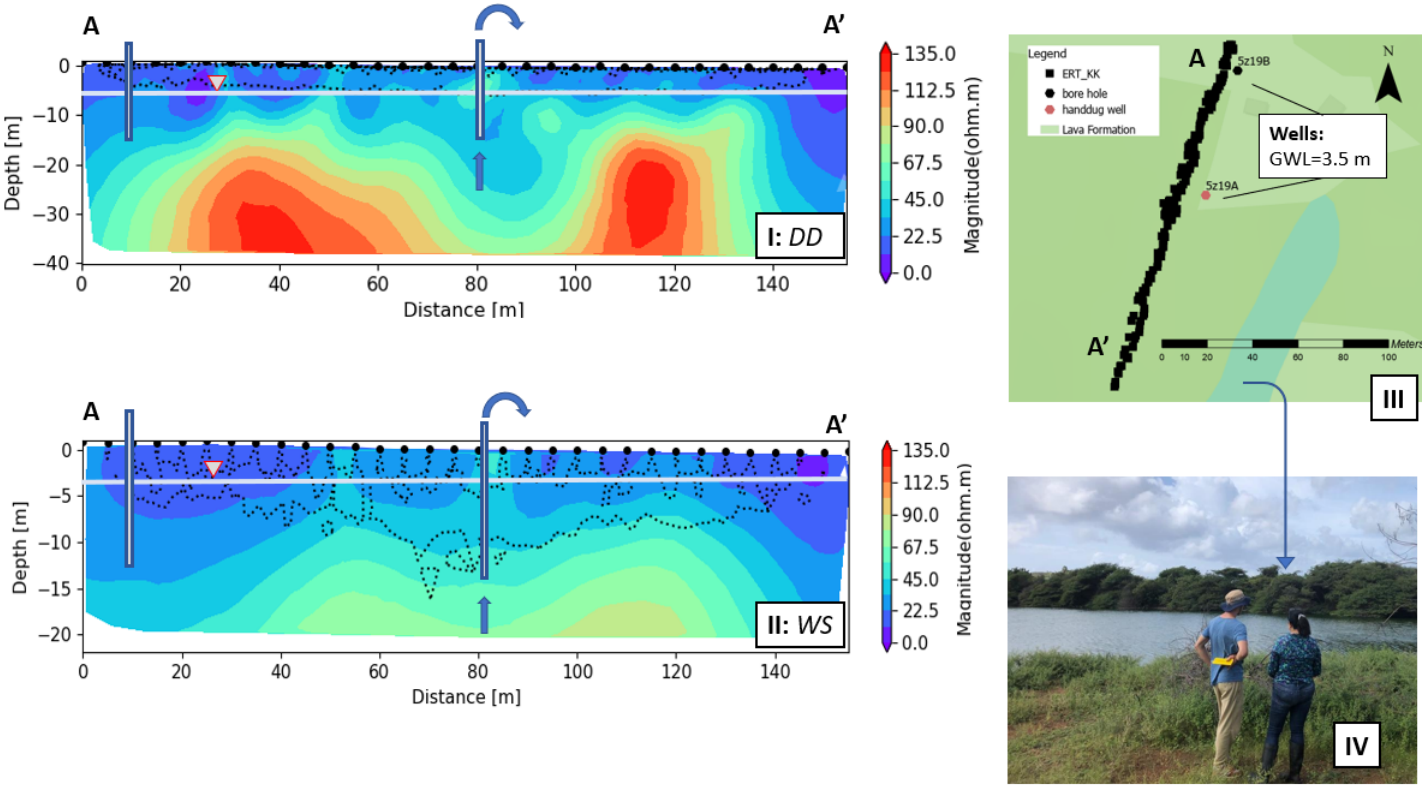

Figure 15: The inversion at Klein Kwartier. **I** is the Dipole-Dipole inversion. **II** below is the Wenner-Schlumberger inversion. **III** shows the local geology, ERT location and well monitoring sites. **IV** a impression of the nearest infiltration pond in Klein Kwartier

4.2 Coastal Transects:

4.2.1 Local Geology

Two ERT measurements were conducted along the coast. One transects was done on the limestone at San Nicolas. Beneath the limestone, Beets described Spaanse Put formation followed by Sint Christoffel formation (Beets, 1977), yet this was not observed in the field, see figure 16. The other transect was done on the lava formation at Pis-

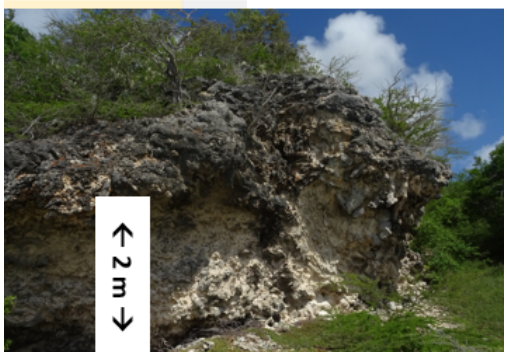

Figure 16: A limestone outcrop at San Nicolas

cadera Bay. The lava formation is the same as found at the inland lava formation sites: pillow basalts; see figure 12.

4.2.2 ERT: San Nicolas *limestone*

At 70 m onwards, there is a layer of high resistivity from 5 to 10 m depth, see figure 17. This is limestone. The limestone layer is discontinuous and between 0 to 70 m distance there is no limestone measured, whilst the outcrop at the beach clearly shows that the subsurface must be limestone, see figure 16. Therefore at the area of low resistivity the limestone has eroded away and filled up with other material over time. Beneath 11 m depth, the resistivity is also very low. This depth coincides with the expected sea level, as The ERT was done at $\approx$ 11 m above the sea. The DOI of the DD is shallower ($\approx$ 5m) than the limestone blowhole and saltwater interface. However, the DOI of the WS is at greater depth ($\approx$ 20m) and includes the above discussed phenomena. Therefore, we can safely assume that at least the salt water interface and the blowhole are indeed present.

4.2.3 ERT: Piscadera Bay *lava formation*

The site is $\approx$ 10 m above sea level. 625 m inland, we measured the at GWL at 11.2 m above sea level. There were signs of surface runoff halfway our transect at 70-110 m distance. The resistivities are relatively low and generally decrease with depth, but the saltwater interface is not as straightforward as at San Nicolas (limestone). The resistivity does drop at $\approx$ 10 m depth, but the transition is more gradual and laterally heterogeneous. Part of the gradual decrease of resistivity with depth can be due to groundwater. The EC of the well was 2.56 mS/cm. This would imply a freshwater lens of at least 1.2 m with a higher resistivity than seawater. The nearby well indicates a fresh/brackish water lens of $\approx$ 1 m thickness. The area of runoff coincides with the location of lower resistivity at the surface: 70-110 m distance, see figures 18 I and II.

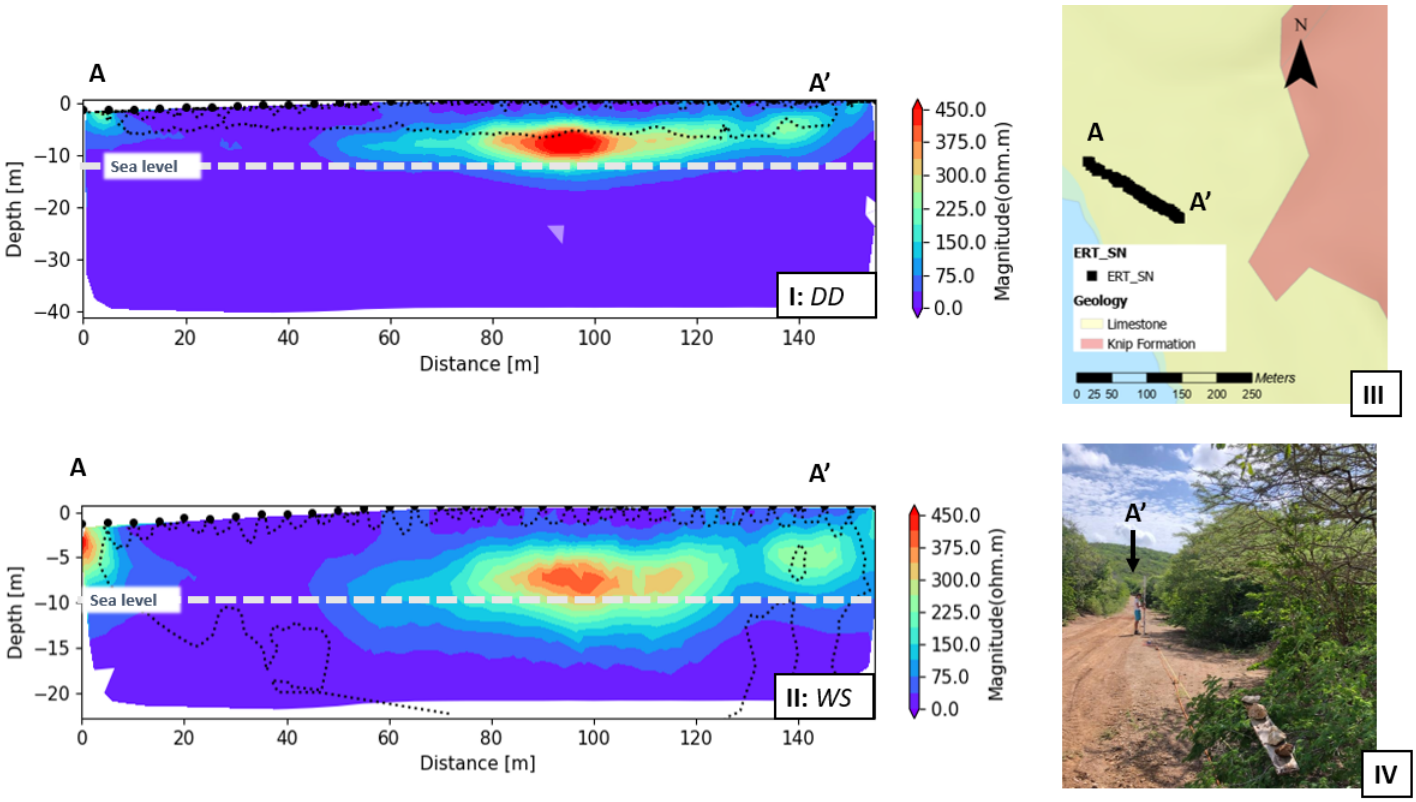

Figure 17: The inversion parallel to the coast at San Nicolas. **I** is the Dipole-Dipole inversion. **II** below is the Wenner-Schlumberger inversion. **III** shows the local geology, ERT location and boreholes. **IV** an impression of the measurement site

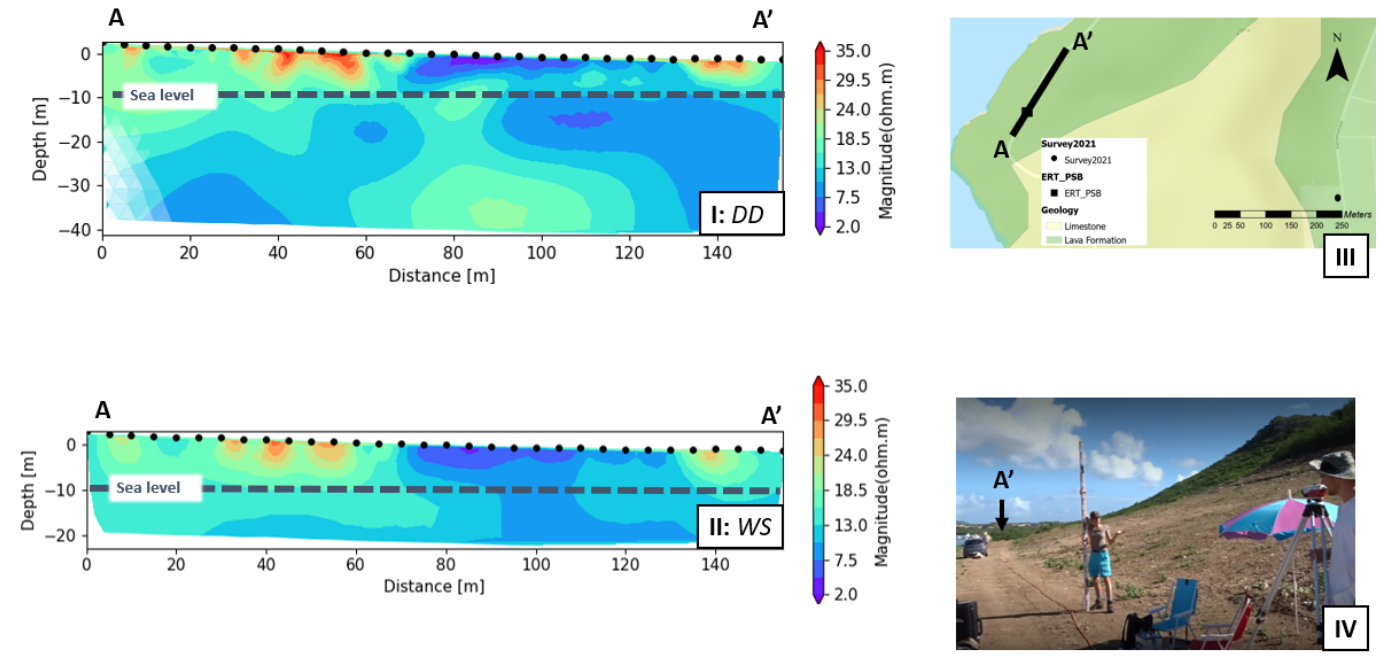

Figure 18: The inversion near the in the inlet of Piscadera Bay. **I** is the Dipole-Dipole inversion. **II** below is the Wenner-Schlumberger inversion. **III** shows the local geology, sea interface & measurement locations. **IV** an impression of the measurement site

4.3 Geological Interfaces:

4.3.1 Local Geology

At Rooi Rincon, there is a limestone outcrop, see figure 19. The underlying midden formation and or lava formation are not visible in the outcrop, yet the lava formation is similar as observed at12. Nearby the Rooi Rincon ERT there is a geological borehole decription of the midden formation: 4N112, see appendix figure 2. Here, the midden formation has alternating layers of limestone (rubble) and silt/clay.

Figure 19: Limestone outcrop in the abrasion gully of Rooi Rincon. Estimated height: 4 m

Ronde Klip had no nearby outcrops, but at the racetrack there is a limestone and midden-formation outcrop. The latter has thinner layers compared to 4N112, see figure 20. Based on field observations the midden formation has a dip of a 38°. The midden formation should be visible in the left (north) side of the ERT profile, where there is a steep increase in elevation. The transect also includes the diorite intrusion and the lava formation. The top layer of the site has been excavated and replaced by dumped rock/rubble. The top layer of the ERT measurement is therefore not in situ material.

4.3.2 ERT: Rooi Rincon *Lava-& Midden Formation*

As the resistivities are very diverse, a log scale is required to capture the heterogeneity. Especially at the surface

Figure 20: Midden formation outcrop at the Race Track

at 100 to 155 m distance there are high resistivities: $\approx$ 1000 $\Omega.m$. Here, we noticed that a thin layer of limestone still persisted at the surface. This is visible in both the DD and the WS inversion. However, the areas of higher resistivity are larger in the WS. In the top left from 0 to 60m distance, there is a horizontal layered structure. In the WS this "confined" area of lower conductivity has a more wavy structure compared to DD. The is because the WS is more sensitive to lateral changes.

The depth of the wavey structure does coincide with the expected water table at 7 m. The GWL was based on interpolation between the groundwater outcrop of Hato spring and GW072 well, see figure 22, therefore it seemed possible that these water sources are connected.

At greater depth, the WS inversion shows 2 areas of high resistivities of around 400 $\Omega.m$. Firstly at 70 m distance at 15 m depth and secondly at 130 m distance at 20 m depth. In between there is an area of lower resistivity of 5- 10 $\Omega.m$. Interestingly, the first area of high resistivity first has a 45 degrees angle with the surface. This coincides with the dip of the midden formation (Beets, 1977), see appendix figure 1. This indicates that the interface of lava and midden formation is located here. Sadly, this is not as apparent in the DD inversion. Again it must be mentioned that the DOI for both inversions is approx 10 m depth. The deeper results are thus quite uncertain.

We created a conceptual model based on the geology map, (Beets, 1977). There was no outcrop in the field to determine the dip direction and angle of the geologies in the field. Based on the DEM of the limestone, we assumed the observed thin layer of limestone to be horizontal. For the Midden formation, used an interpolation of the dips observed by Beets, see appendix figure 1. Initially we did include the water table in the forward model, but it had no impact on the results of the forward model and therefore it was left out. The resistivity of the formations according to Archie's law were very high, far higher

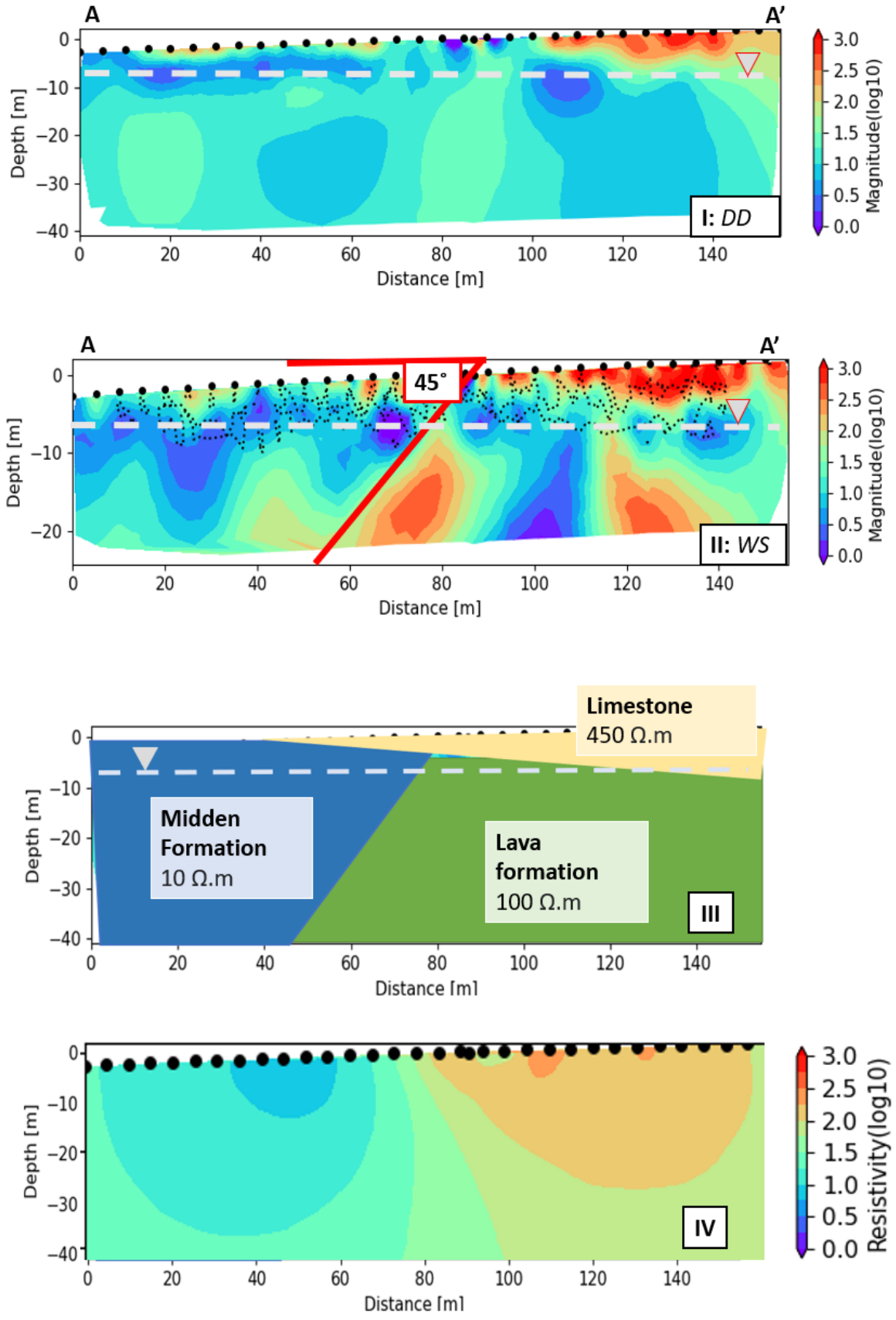

Figure 21: The inversion of the Rooi Rincon ERT. **I** is the Dipole-Dipole inversion. **II** below is the Wenner-Schlumberger. **III** The conceptual model of Rooi Rincon. **IV** The results of the forward model based on the results

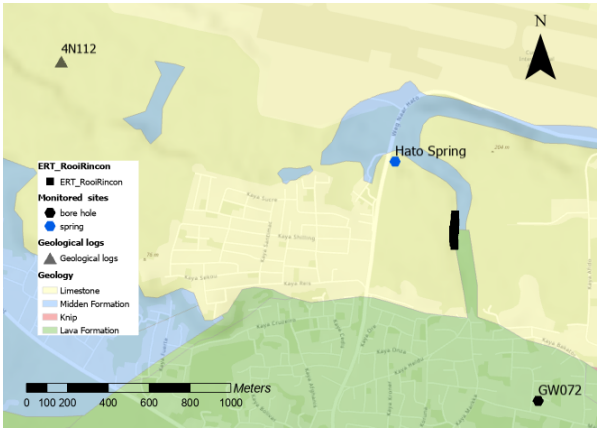

Figure 22: An overview of the Rooi Rincon ERT transect including the location of Hato spring, well and geological borehole.

than observed in the inversion model: 167 & 1000 Ω.m. (saturated and unsaturated lava formation), 3770 Ω.m. (unsaturated limestone) and 421 & 26540 Ω.m. (saturated and unsaturated midden formation). These values are so high, especially for unsaturated rock, that we used the resistivies measured in the inversion as input for the forward model. The conceptual model and the resulting forward model are shown in figure 21 III and IV.

4.3.3 ERT Ronde Klip *Diorite intrusion*

From left to right, the ERT measurement should show midden-formation, the diorite intrusion followed by basalt. The measured EC of the groundwater fluctuated between 6.1 and 8.7 mS/cm, thus the water is brackish as the caretaker said. This was measured in a well of approx. 10 m deep with the water table at ≈ 6.4 m depth. The DD inversion had many inversion errors, see appendix figure 3, and therefore many measurements were filtered resulting in the very smooth inversion seen in figure 23 I. Thus, the DD inversion should be treated with care. The WS inversion has no errors.

A sharp increase in resistivity is encountered at 10-15 meters depth. Here, the resistivity increases from 5-10 $\Omega.m.$ to 100 $\Omega.m.$ and more. The high resistivity is most likely the intrusion and its magnitude coincides with the intrusion measured at the race track, see 24. Above the intrusion, resistivities are low: +- 10 ohm, reaching as low as 3 $\Omega.m$ at expected the water table. This cover layer consist of most likely of eroded material (clay) deposited after a rainfall event, as this area functions as a rooi. Alternatively, the intrusion has not broken through the lava formation and the area of low resistivity is highly weathered basalt.

4.3.4 ERT Race Track *diorite intrusion*

From north to south we should encounter the midden formation, followed by the intrusion and than the lava formation. The GWL was measured to be at 15m depth in a nearby well. Assuming the groundwater table follows the local elevation, the groundwater should be at ≈. 22 m depth. The intrusion can be seen at 10 m depth, see figure 24 similar to Ronde Klip. Here the DD inversion is of better quality and is more trustworthy. We placed the first two ERT pins in the midden-formation. At these pins we see a slight change in resistivity at the surface till 5 m depth, this is especially apparent in the WS inversion. The intrusion does not seem to reach the surface. The area of high resistivity associated with the diorite is located at $>$ 5 m depth. The *assumed* groundwater table somewhat coincides with the depth of the intrusion at $>$60 m distance, but no clear decrease in resistivity can be observed.

To testify the width of the intrusion at the race track, we created a forward model. The groundwater is brackish: 8.0 mS/cm, however the resistivities according to the laws of Archie were still too high: 31 & 1980 $\Omega.m.$ (saturated and unsaturated lava formation), 3125 & 312500 $\Omega.m.$ (saturated and unsaturated diorite) and 103 & 6520 $\Omega.m.$ (saturated and unsaturated midden formation). Therefore, we inferred the resistivities from the inversion. The conceptual model and resulting forward model are shown in figure 25 I and II. After trial and error, and trying different intrusion widths, we saw no significant difference in forward model results. Thus, do not know how wide the intrusion is in the subsurface.

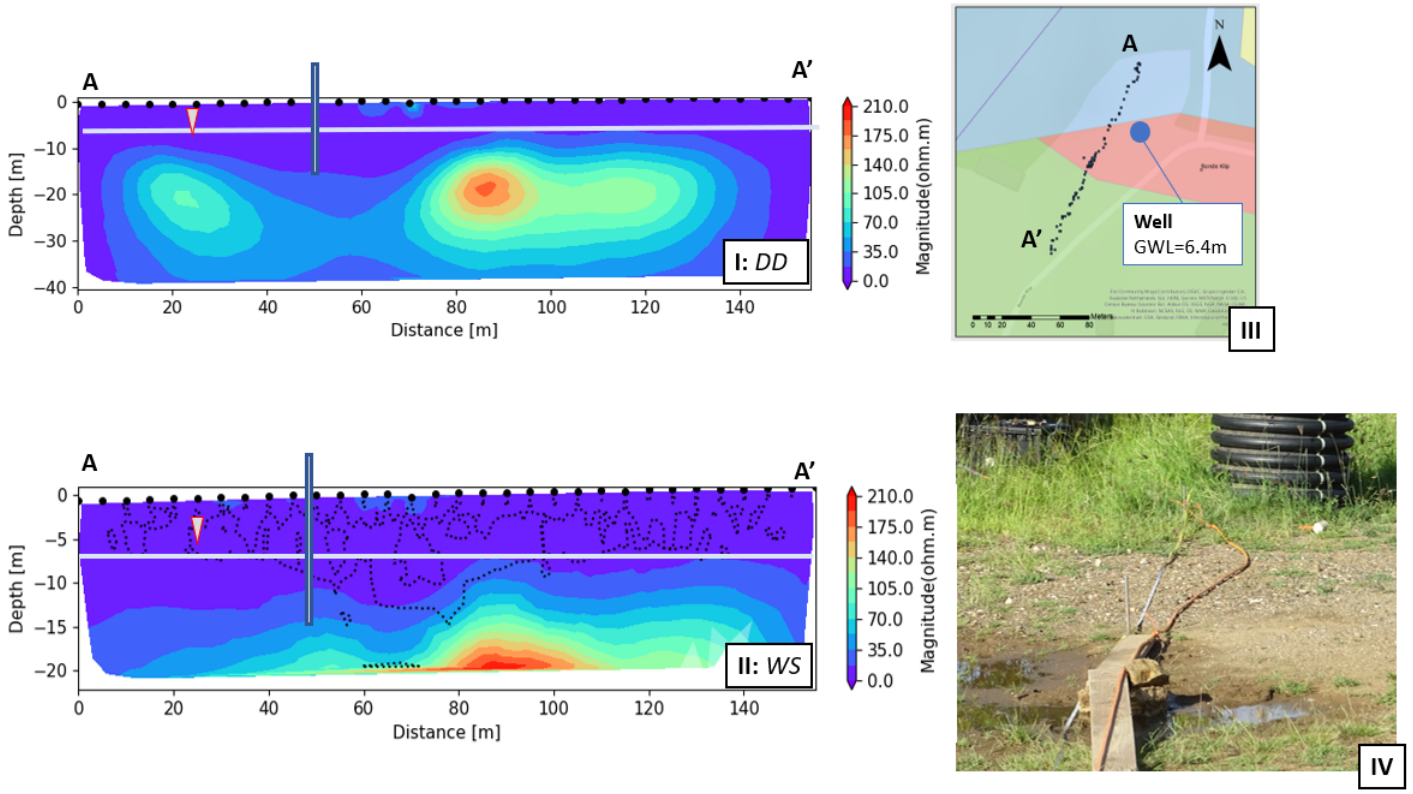

Figure 23: The inversion at near Ronde Klip. **I** is the Dipole-Dipole inversion. **II** below is the Wenner-Schlumberger inversion. **III** shows the local geology, ERT location and groundwater monitoring site. **IV** an impression of the measurement site

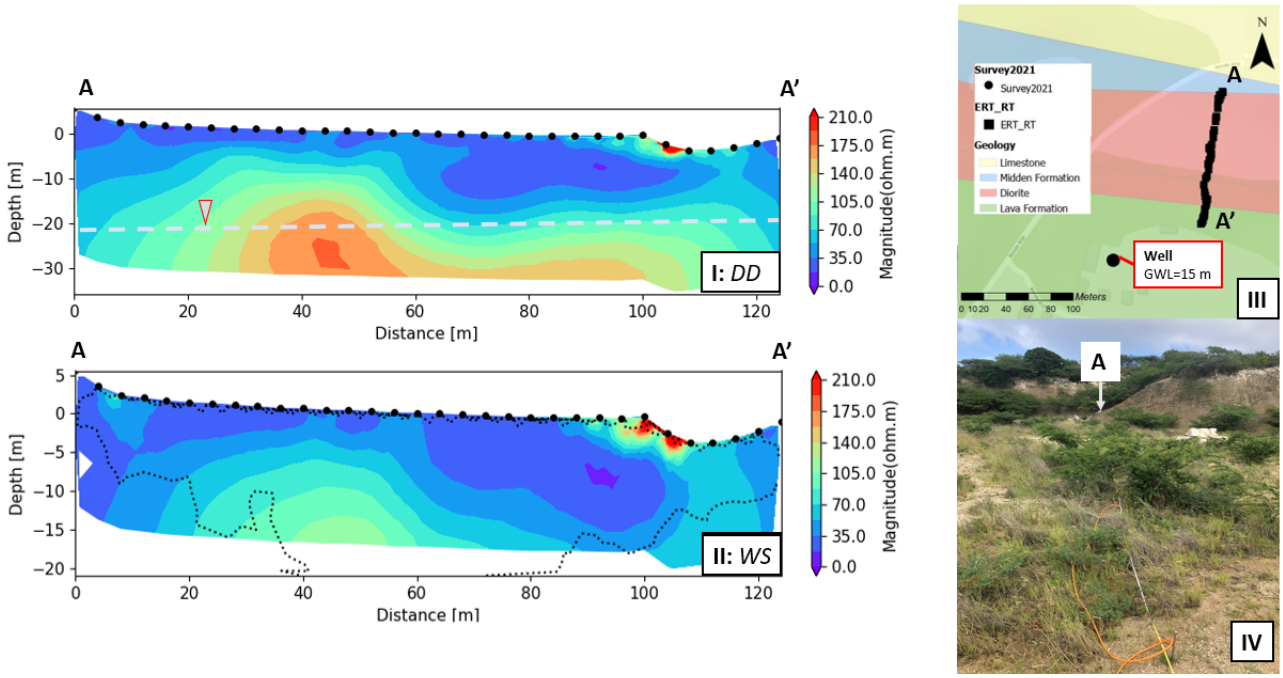

Figure 24: The inversion at near Ronde Klip. **I** is the Dipole-Dipole inversion. **II** below is the Wenner-Schlumberger inversion. **III** shows the local geology, ERT location and groundwater monitoring site. **IV** an impression of the measurement site

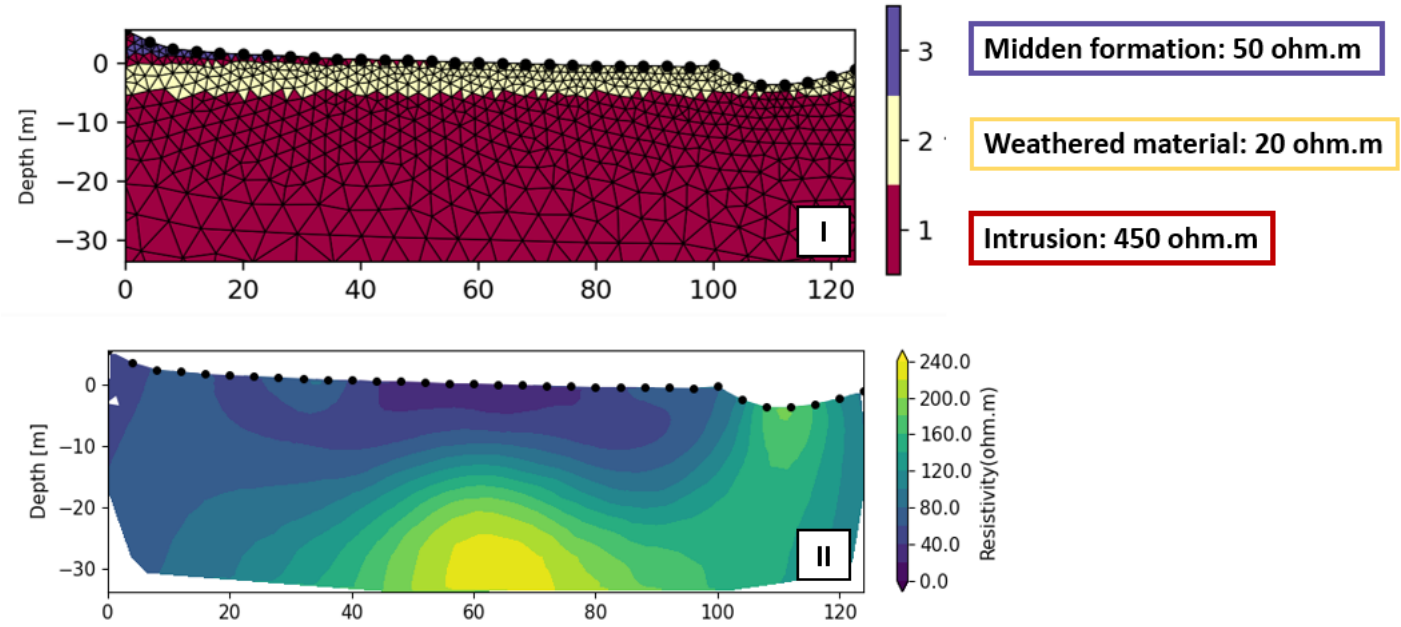

Figure 25: **I** The conceptual model of Race Track. **II** The results of the forward model

4.4 Groundwater measurements and Monitoring wells

4.4.1 Singular measurements

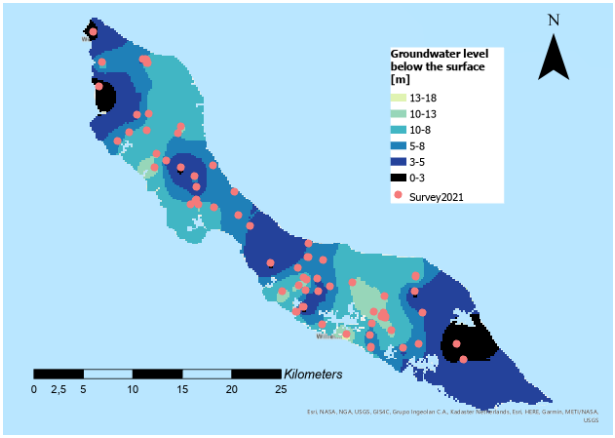

Figure 26: A kriging map of the groundwater level below the surface (m) based on the 2021 GWL measurements

Based on the DEM and singular measurements of the groundwater level in 2021, we computed both a map of the groundwater level below the surface (m) and above sea level (m), see figure 26 and 27. The spatial accuracy of the maps are not very high, yet they give an indication of the general groundwater flow and bulge. The groundwater level below the surface is the deepest at the north-south anticlines, see figure 26. It seems that the groundwater flow is predominantly towards west coast, see figure 27.

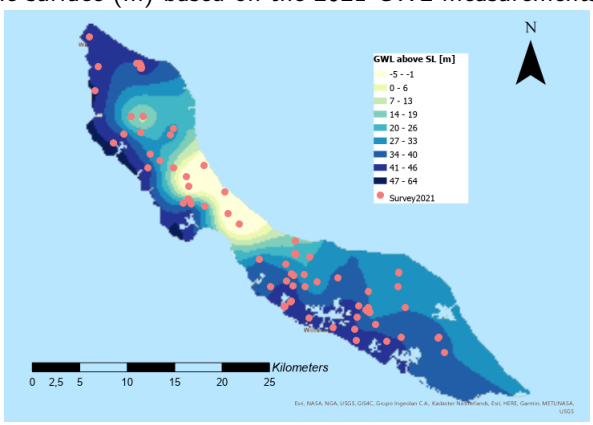

Figure 27: A kriging map of the groundwater level above sealevel (m) based on the 2021 GWL measurements

4.4.2 Monitoring wells

Figures 28 and 29 show the normalized groundwater levels over time. *GW002*, *GW029*, and *GW077* show strong temporal variation in GWL, see 28. In the case of *GW002*, the fluctuation is caused by pumping. At *GW029* well the data from 02/11/2021 till 07/12/2021 does not reflect the groundwater behavior. We discovered that the well acted as a drain for the ponding rainwater at the surface. This caused $\approx$ 5 m increases in groundwater level. When we discovered this unwanted drainage pattern, we created a small earthen dam around the well. For *GW077* we see a similar jump in GWL. Yet, this well was properly covered, so its more likely that the (extreme) rain event during the measurement: 18.9 mm is the sole cause of the increased GWL.

During the monitoring period in the eastern side of the island, we can clearly see an increase in groundwater level over time, see figure 29. *GW029* well, located in the center of the island but plotted here as a reference, shows a similar increase in groundwater level. *GW014*, *5Z19A* and *5Z19B* are located close together and show very similar increase in groundwater level, with the exception of the sudden drop in water level of *5Z19B* at 05/11/2021 due to the pumping. *GW006* on the other hand does not follow the same trend as the other wells.

All wells, except GW002, show an increase in GWL after the great rain event on 02/12/2021. Thus, we computed the slopes (cm/d) of the increase in groundwater level around this period, for precise times see table **??** in the Appendix. In figure 30, we can see that the GWL at *GW077* reacts at least twice as fast than the other

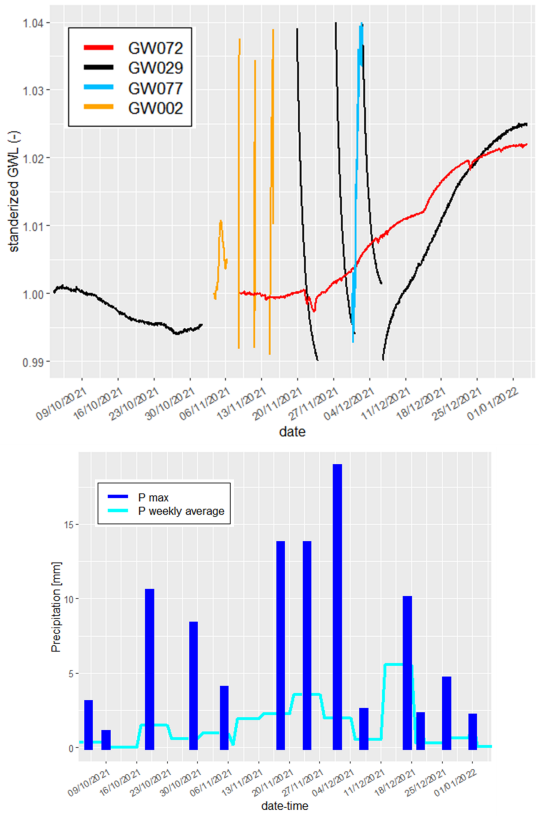

Figure 28: **Top panel:** The normalized groundwater level at the center of the island. The measured groundwater levels have been corrected for barometric pressure and erroneous measurements have been filtered out. **Bottom panel**: Rain data from Hato airport

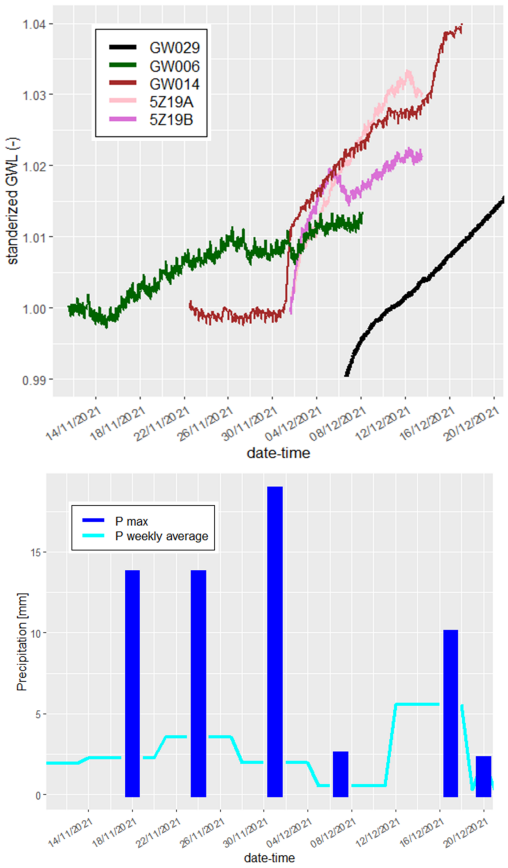

Figure 29: **Top panel:** The normalized groundwater level in the eastern part of the island. The measured groundwater levels have been corrected for barometric pressure and erroneous measurements have been filtered out. **Bottom panel**: Rain data from Hato airport

monitoring sites. Followed by the **un-pumped** *5Z19B*. *GW014* and *5Z19A* react similarly. The same goes for *GW006*, *GW029* and *GW072*. Only after pumping, does the slope of *5Z19A* drop drastically.

Table 6 shows the general statistics of the monitored groundwater sites. Some time after the start of the measurement period, the wells *GW002* and *5Z19A* experienced pumping, hence the large σ in (m). Interestingly enough, well *5Z19B* which is located right next to *5Z19A* has the lowest variation in GWL. It seems it has been very little effected by the nearby pumping.

Table 6: A summary of the basic statistics of the GWL (m) in the monitoring wells. These values have been filtered and adapted to sealevel prior to computation. All values are in meters above SL.

	GW072	Mark	GW077	GW002	GW006	GW014	5Z19A	5Z19B
Min.	38.50	13.62	2.60	4.56	15.83	9.86	9.01	11.61
1st Qu.	38.63	14.03	5.03	4.94	17.82	13.17	11.75	11.80
Median	39.06	14.08	5.13	5.26	17.90	13.47	11.85	11.82
Mean	39.06	14.11	5.10	5.65	17.88	13.44	11.80	11.81
3rd Qu.	39.45	14.23	5.20	6.48	17.94	13.58	11.94	11.85
Max.	39.52	14.47	5.24	6.97	18.01	13.79	11.98	11.88
σ	0.36	0.19	0.20	0.79	0.09	0.25	0.33	0.05

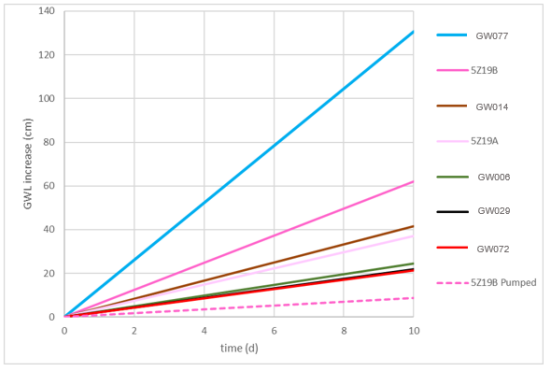

Figure 30: The increase in GWL over time (cm/d) per well after the high rainfall event on 02/12/2021

4.5 Hato spring

For Hato spring the EC_{bg} was around 1.5 mS/cm and we estimated the discharge to be 1.5 l/s. As mentioned in the method section, the measurement set-up was subjected to trial and error. The size of the marionette and ΔEC differed per measurement, see appendix table 2.

Appendix table 8, also contains the plots to visually determine the other required parameters. The wet area, A, was on average 0.4885 dm^2. Table 7 below shows the velocity of Hato spring and the discharge measured using both methods. The discharges Q_{dil} and Q_{velo} are in the same order of magnitude. Q_{dil} is more stable with an average of 0.63 ($\pm$ 0.06) l/s, whereas Q_{velo} has an average of 0.64 ($\pm$ 0.16) l/s. The average velocity v is 1.31 ($\pm$ 0.33) m/s.

Table 7: Timestamp, measured discharge via dilution method and measured velocity and discharge via peak method.

Date Time	Q_{dil} *(l/s)*	v *(m/s)*	Q_{velo} *(l/s)*
19/11/2021 13:55	0.59	0.95	0.47
22/11/2021 16:56	0.62	1.47	0.72
26/11/2021 17:07	0.58	1.69	0.83
30/11/2021 17:39	0.72	1.12	0.55

5 Discussion

5.1 Inland Lava Formation

The higher porosity in the rims of the basalt and the gradual decrease in weathering explains the hydrological heterogeneity within the pillow lava formation

All ERT measurements of the inland lava formation are very patchy. This can be explained by the different degree of weathering of the lava formation. As we noticed in the outcrops of the lava formation, the pillows of the basalt have fractured rims. However, the patches of high resistivity in the ERT are larger than what can be contributed to the weathering of *one* pillow basalt. The diameter of one pillow basalt is $\approx$ 0.5 to 1 m, with the hard core the size of a football. Whereas the patches of high resistivity have a diameter of $\approx$ 10 m. Thus, it is more likely that there are clumps of pillow basalt that are less weathered and thus have a higher resistivity. These clumps of pillow basalt form (small) barriers for groundwater flow. This explains the variability groundwater availability between wells in the Parallele weg neighbourhood.

Because the weathering of the lava formation decreases with depth, there should be a base with the same resistivity as these clumps of unweathered pillow basalts. Based on borehole descriptions, this base is 26m below the surface. Only at Klein Kwartier we observed a semi-continuous base of higher resistivity that was somewhat continuous at $\approx$ 20 m depth. This coincides with the remark of G.H.J. Molengraaf (1929) that at Klein Kwartier diabase not thoroughly weathered. At the other two locations the aquifer base was not observed in the ERT inversions.

At the surface and in between the aforementioned clumps of unweathered pillow basalt the measured resistivity is low. The measured resistivty (5-10 $\Omega.m$) matches with the value found for clay at PortoMari, see table 2. This makes sense as clay is a weathering product of basalt (Singer, 1970). Therefore, it is clay that has either weathered in-situ or been washed. In addition or alternatively, the lower resistivity is (partly) caused by groundwater through the more weathered patches.

An odd ball out is the is the sudden drop in resistivity below the pumped well of Klein Kwartier. If pumping caused the lower and the The reason behind this is unclear.

5.2 Coastal transects

The limestone is far more penetrable for seawater. In the transect we did, the limestone did not form any barrier for seawater intrusion. In the inversion we did notice a discontinuity within the limestone terrace. During an episode of higher sealevels, a blowhole must have formed here. Similar to those observed on the north coast of Curaçao today: Watamula and Boka Pistol. This blowhole was later filled up with clay alluvium from runoff which have a lower resistivity.

The lava formation forms a better barrier against seawater intrusion. However, the heterogenous nature of the lava formation means that in some areas are more permeable for (salt) water and will allow for salt water intrusion further inland. That is why in figure 18 I and II, there are patches of very low resistivity (seawater intrusion) and patches of higher resistivity below the sea-level.

5.3 Geological Interfaces

5.3.1 Midden-, lava formation and Hato spring

Based on the ERT at Rooi Rincon, the groundwater does not seem to penetrate deep into the midden formation. Some layers within the midden formation seems more penetrable and the aquifer is max 10 m deeper here. However, the patchiness of the weathering in the lava formation (pillow basalt) does allow deeper penetration of the groundwater. It seems that at the interface of these two formations at Rooi Rincon part of the groundwater seeps into deeper layers, whilst the other part seeps into the shallow, more weathered part of the midden formation. There it travels north until there is a groundwater outcrop: Hato spring. Conceptually, this would look like figure 31. *Note, we unsuccessfully tried to prove the geological structure, interface and dip of midden formation, with a forward model.*

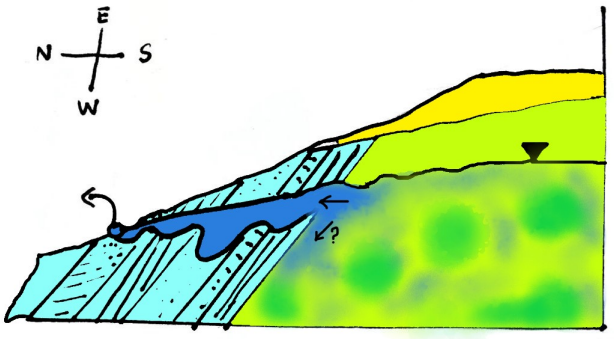

Figure 31: Conceptual model of groundwater flow towards Hato sping. Light blue is the midden formation, green the lava formation, yellow the limestone and dark blue the groundwater.

It would be logical to assume that the groundwater only enters the midden formation when the lava formation "bucket" overflows. But this would mean that during dry periods, there is limited flow into the midden formation

and Hato spring would run dry. Yet, Hato spring is one of the few springs on the island with a year-round discharge, see table 2 in Appendix. Thus, the midden formation "conduit" must always be located below the GWL.

Others believe that Hato spring is fed by rainwater that penetrates the limestone, hits the dipped midden formation and is then transported to Hato spring (Abtmaier, 1978), (Molengraaff, 1929). This theory is based on the high infiltration capacity of limestone, not on storage capacity (Henriquez, 1962). In the field, we observed cracks and caves, which are conduits for groundwater flow. Similarly, the San Nicolas ERT on the limestone showed strong saltwater intrusion, which also indicates high permeability. So, if the limestone has little storage capacity, the theory of Molengraaff and Abtmaier would also result in a strongly fluctuating and discontinuous spring discharge.

Also, the EC of Hato spring is similar to that of GW072 well located in the lava formation, south of Hato spring. Therefore, it is most likely that the lava formation forms the reservoir for the Hato spring and that the midden formation only forms a conduit.

5.3.2 Diorite intrusion

We think the diorite intrusion is impermeable for water based on the following three observations: (1) at both Ronde Klip and the Race Track the intrusion has a high resistivity, (2) the very low porosity measured for the diorite and (3) the rock is very hard (dynamite was required to remove it for construction), thus weathering is an even slower process. The low permeability of the intrusion means it forms a barrier for groundwater flow: a dyke.

The width of the diorite intrusion cannot be determined from the ERT inversions. It was proven with forward modelling that under the surface the intrusion could extend further north and south than implied by Beets geology map. Based on Beets map, the intrusion is $\approx$ 100 m wide. This is thus the *minimum* expectable width.

The maximum height of the intrusion differs at the two ERT locations. At Ronde Klip the intrusion is at 19 m above sea level (12m below surface), whilst at the Race track the intrusion is reached 42 m (5 m below surface) above sea level. The height of the dyke thus decreases dips eastward, towards Ronde Klip, with an angle of 0.6.

The wells surrounding the intrusion are very brackish. According to one local, this area is referred to as the “salt highway” in Papiamentu (RESULTS). We did indeed measure higher EC in the wells next to the diorite intrusions. At Ronde Klip: 6.1 mS/cm and at the Race track 8.0 mS/cm. It is illogical that the increased salinty is caused by seawater intrusion as both well are located inland of the non-permeable diorite dyke. A more sensible cause is the presence of fossil seawater. The fossil seawater is either (I) in the thin layer of Ronde Klip formation (midden formation) inland of the diorite intrusion or (II) in the lava formation or (III) both. Both layers were formed under submarine conditions and experienced multiple periods of re-submersion. Generally, the midden formation has experienced the least freshening due to its lower permeability, (Abtmaier, 1978), yet based on the southward groundwater flow see figure 26, the lava formation will not have experienced much freshening either.

We initially tried to reproduce the ERT inversions with Forward models based on Archies equations. However, the values computed were too high, especially for the unsaturated zone. The most likely causes are (I) the clay from weathered basalt and (II) salt. The clay is either deposited at the surface (alluvium) or is located between the pillow basalts via in-situ weathering processes. The salt is either fossil (at depth) of from salt spray. Both processes decrease the resistivity of the geological formation, but where not taken into account when computing the laws of Archie.

5.4 Groundwater measurements and monitoring

The high rainfall event on 02/10/2021 has most likely caused the increase in groundwater monitored in that period. Based on the increase in groundwater level (GWL) over time, we can group the monitored groundwater levels into 4 groups from a high to low response in groundwater increase.

1. The GWL at GW077 increase the quickest. A possible explanation is that this well is located at the end of a rooi in the lava formation. The groundwater in this area is generally shallow, see figure 26. Another explanation would be a low storage coefficient caused by a thin aquifer, low porosity, ect. However, GW077 well is adjacent to geological borehole decriptions (Abtmaier, 1978) and the Centrum Piscadera supermarket ERT transect. Both data sources show no indication of shallow(er) aquifers than at the other monitoring sites. Thus, the steep increase is most likely caused by topography.

2. 5Z19A (pre pumping) has the second highest increase in GWL over time. One would expect it to be the same as 5Z19B and GW014, due to their proximity. Yet the latter two react slightly slower to the rain fall event. We don’t think the discrepancy is caused by the infiltration, for in that case 5Z19B would have the same slope. From the ERT in the Klein Kwartier transect, see figure 15, we can see that the subsurface below 5Z19A is very odd. What

the cause of the irregular subsurface is, is unclear, but it might be an explanation for this situation.

3. GW014 and 5Z19B. Their similarity makes sense as they are very close to each other, experience no pumping and are in the same geological formation.

4. GW072, Mark and GW006 form the last group with the slowest response to rainfall. The wells of Mark and GW072 are both in the lava formation and in close(r) proximity of each other. Whereas GW006 is located in the midden-formation and diorite intrusion. Their similarity can therefore be arbitrary or be caused by topography. All three locations are on/near local elevated areas. In addition the wells are located on the edge of the water bulge. Therefore, there the groundwater recharge is lower and the response slower. The lower groundwater recharge flux also confirms the hypothesis that the lack of freshening is what caused the higher EC values at GW006 and the Race Track, see 6.3.

Based on the time serie data of 5z19A and 5Z19B, it seems that wells in the lava formation are hardly effected by nearby pumping, see chapter *5.4.2*. Of course, we must take into account that these wells are located next to the infiltration ponds of Klein Kwartier. Therefore, the extra water input may have buffered the pumping effect.

5.5 Hato Spring

In November 2021 the average measured discharge of Hato spring was lower than any measurement done by Abtmaier in 1976, 1977 and 1978, see appendix figure 2. In the late 1970's the average discharge was 0.78 ($\pm$ 0.25) l/s, compared to the average 0.63 ($\pm$ 0.06) l/s we measured in 2021. It is unlikely that the discrepancy originates from different rainfall conditions, as Abtmaier stressed that he measured during 3 consecutive dry years, and 2021 was a relatively wet year with November being the wettest month, see figure 28. From the meteorological point of view the discharge should have increased. Instead the discharge of Hato spring has decreased compared to 50 years ago. Where the "missing discharge" has gone, is debatable. Maybe the drainage pattern of Hato springs has changed due to increased (concrete) surface runoff, leading to less infiltration of rainwater. Alternatively, pumping in nearby wells has increased, reducing the groundwater level of the reservoir.

6 Conclusion

The lava formation is a patchy aquifer. The permeability depends on the extent of weathering, which is laterally heterogeneous, but also generally decreases with depth. The aquifer base (e.g. unweathered lava formation) has not been observed in the ERT measurements, but based on Abtmaiers geological borehole descriptions, the aquifer is at least 26 m deep, (Abtmaier, 1978). The lateral heterogeneity in weathering is due to structure of the lava formation: pillow basalt. Some clumps of pillows are less weathered, forming obstacles for groundwater flow.

As a result of the heterogeneous permeability, the extent of seawater intrusion in the coastal lava formation is strongly variable. Yet, the lava formation forms a better barrier for sea-fresh water mixing than the limestone terraces. Based on both the ERT measurements and high EC measurements in the limestone (Abtmaier, 1978), the limestone forms a conduit for seawater intrusion. Whereas for the coastal lava formation at 625 m inland the groundwater is relatively sweet. Groundwater flow is hampered to some extent at geological interfaces. Groundwater overflows from the lava formation reservoir into the shallow, more weathered, part of the midden formation. At Rooi rincon, the midden formation forms a conduit of continuous groundwater from the lava formations. This explains why Hato spring is one of the few continuous springs on Curaçao. The diorite intrusion is an aquitard. It forms a groundwater dyke and thus hampers both groundwater flow and seawater intrusion through the limestone. Inland of the intrusion, the groundwater is very brackish due to little freshening of lava formation aquifer and/or fossil seawater.

Thus, the lava formation forms the main aquifer of the island, yet the surrounding midden formation and diorite intrusion contain the groundwater within the lava formation. If the same occurs at the interfaces with the knip formation is unknown and should still be researched. The limestone does not form a barrier for water flow and has no storage capacity, therefore when the lava formation is in direct contact with limestone, it will leach through the limestone into sea.

Spatially, groundwater flows from north-east coast towards the south-west coast. Based on the change GWL over time, the behavior of GWLs is predominantly determined by topographical location and pumping. The GWL in the rooi experiences rapid increase after a rainfall event as is located in an accumulation area for rainwater. Thinner aquifers and additional wastewater input also result in a fast GWL response to rainfall. Whereas on topographically higher areas, groundwater response is slowest. These results indicate that for the lava formation, we can assume a topographical water divide.

As the lava formation is an aquifer and forms the predominant surfacing geology, it will most likely experience the most leaching of nutrients and other solutes to the groundwater. These solutes may threaten for coral health. Therefore, for future SGD research we would advise to focus on the areas along the south-west coast where the lava formation is in direct contact with the sea or limestone. Here seaward groundwater flow is not hampered by the midden formation or the intrusion and thus forms hot spots of Submarine (polluted) Groundwater Discharge.

References

Abtmaier, B. (1978). *Zur Hydrogeologie der Insel Curacao : (Niederlaendische Antillen)* (Doctoral dissertation, Aachen). Retrieved from https://publications.rwth-aachen.de/record/67375 (Aachen, Techn. Hochsch., Diss.)

Archie, G. (1942, 12). The Electrical Resistivity Log as an Aid in Determining Some Reservoir Characteristics. *Transactions of the AIME*, *146*(01), 54-62. Retrieved from https://doi.org/10.2118/942054-G doi: 10.2118/942054-G

Archie, G. E. (1952). Classification of carbonate reservoir rocks and petrophysical considerations. *Aapg Bulletin*, *36*(2), 278–298.

Beets, D. (1972). Lithology and stratigraphy of the cretaceous and danian succession of curaçao.

Beets, D. (1977). Cretaceous and early tertiary of curaçao. In *8th caribbean geological conference. amsterdam, geophysical union of america, papers of geology, guide to field excursions* (Vol. 10, pp. 18–28).

Beets, D., De Buisonje, P., & van Verkhoven, C. (1977). Geologische kaart van het eiland curacao n.w.i.

Blanchy, G., Saneiyan, S., Boyd, J., McLachlan, P., & Binley, A. (2020, 02). Resipy, an intuitive open source software for complex geoelectrical inversion/modeling. *Computers Geosciences*, *137*, 104423. doi: 10.1016/j.cageo.2020.104423

Burke, L., Reytar, K., Spalding, M., & Perry, A. (2011). *Reefs at risk revisited*. World Resources Institute.

Castrechini Rodriguez, A. F. (2021). Relationship between land characteristics and coral reefs in curacao. *Wageningen Marine Research, Wageningen University and Research*.

CBS. (2021, Apr). *Climate*. Central Bureau of Statistics Curaçao. Retrieved from https://www.cbs.cw/climate

de Buisonjé, P. H. (1974). Neogene and quaternary geology of aruba, curaçao and bonaire. *PhD thesis, Universiteit van Amsterdam*.

Developers, G. (n.d.). *Electrical conductivity of rocks¶*. Retrieved from https://gpg.geosci.xyz/content/physical$_p roperties/tables/electrical_c onductivity.html$

Erdogan, E. (2021). *The terrestrial consequences of poor wastewater management in curaçao: How exploring public health risks and ground water quality levels can provide insights into establishing its sustainable management for small island development states* (Unpublished master's thesis).

Glover, P. (2009). What is the cementation exponent? a new interpretation. *The Leading Edge*, *28*(1), 82–85.

Glover, P. (2015). 11.04–geophysical properties of the near surface earth: Electrical properties. *Treatise geophys*, 89–137.

Grontmij, & Sogreah. (1968). Water and land resources development plan for the island of aruba, bonaire and curacao.

Henriquez, P. (1962). Problems relating to hydrology, water conservation, erosion control, reforestation and agriculture in curacao. *New West Indian Guide / Nieuwe West-Indische Gids*, *42*(1), 1 - 54. Retrieved from https://brill.com/view/journals/nwig/42/1/article-p1$_3 .xml$ doi: https://doi.org/10.1163/22134360-90002318

Hippolyte, J.-C., & Mann, P. (2011). Neogene–quaternary tectonic evolution of the leeward antilles islands (aruba, bonaire, curaçao) from fault kinematic analysis. *Marine and Petroleum Geology*, *28*(1), 259-277. Retrieved from https://www.sciencedirect.com/science/article/pii/S0264817209001214 (Thematic Set on: Tectonics, basinal framework, and petroleum systems of eastern Venezuela, the Leeward Antilles, Trinidad and Tobago, and offshore areas) doi: https://doi.org/10.1016/j.marpetgeo.2009.06.010

Hongve, D. (1987). A revised procedure for discharge measurement by means of the salt dilution method. *Hydrological processes*, *1*(3), 267–270.

Johnson, T. C., Day-Lewis, F. D., & Slater, L. (2020). *electrical imaging for hydrogeology*. Guelph, Ontario, Canada: The GROUNDWATER PROJECT. Retrieved from https://gw-project.org/books/electrical-imaging-for-hydrogeology/

Kambesis, P., Mylroie, J., Mylroie, J., Larson, E., Owen-Nagel, A., Sumrall, J., & Lace, M. (2016, 01). Influence of karst denudation on the northwest coast of curacao.

Kerr, A. C., Tarney, J., Marriner, G. F., Klaver, G. T., Saunders, A. D., & Thirlwall, M. F. (1996). The geochemistry and petrogenesis of the late-cretaceous picrites and basalts of curaçao, netherlands antilles: a remnant of an oceanic plateau. *Contributions to Mineralogy and Petrology*, *124*(1), 29–43.

Klaver, G. T. (1987). The curaçao lava formation: an ophiolitic analogue of the anomalous thick layer 2b of the mid-cretaceous oceanic plateaus in the western pacific and central caribbean.

Klimaatinfo. (2021). Retrieved from https://klimaatinfo.nl/klimaat/nederland/

Loewen, M. W., Duncan, R. A., Kent, A. J. R., & Krawl, K. (2013). Prolonged plume volcanism in the caribbean large igneous province: New insights from curaçao and haiti. *Geochemistry, Geophysics, Geosystems*, *14*(10), 4241-4259. Retrieved from https://agupubs.onlinelibrary.wiley.com/doi/abs/10.1002/ggge.20273 doi: https://doi.org/10.1002/ggge.20273

Loke, M. H. (2004). *Tutorial: 2-d and 3-d electrical imaging surveys.* Birmingham, UK.

Lubarsky, K. A., Silbiger, N. J., & Donahue, M. J. (2018). Effects of submarine groundwater discharge on coral accretion and bioerosion on two shallow reef flats. *Limnology and Oceanography*, *63*(4), 1660–1676.

Meteo.cw. (2010). Retrieved from https://www.meteo.cw/climate.php?Lang=EngSt=TNCCSws=R11

Molengraaff, G. J. H. (1929). Geologie en geohydrologie van het eiland curaçao.

Moore, j. v. n. p. y. p., RD et al. (n.d.). Introduction to salt dilution gauging for stream flow measurement part 2: Constant-rate injection.

Morgan, F., Coles, D., Vichabian, Y., & Sogade, J. (2001). Assessment of the groundwater resources at plantages portomari, curacao. part iii: Final report.

Muhs, D. R., Pandolfi, J. M., Simmons, K. R., & Schumann, R. R. (2012). Sea-level history of past interglacial periods from uranium-series dating of corals, curaçao, leeward antilles islands. *Quaternary Research*, *78*(2), 157-169. Retrieved from https://www.sciencedirect.com/science/article/pii/S0033589412000555 doi: https://doi.org/10.1016/j.yqres.2012.05.008

OHI. (2017). *Coral reefs.* Retrieved from http://www.oceanhealthindex.org/methodology/components/coral-reefs

Qi, Y., Ghorbani, A., Gresse, M., & Thomas, D. (2021, 01). Induced polarization of volcanic rocks. 5. imaging the temperature field of shield volcanoes. *Geophysical Journal International*, *225*. doi: 10.1093/gji/ggab039

SEALINK. (n.d.). *The sealink project.* Retrieved from https://www.sealinkcaribbean.net/

Seo, S. B., Mahinthakumar, G., Arumugam, S., & Kumar, M. (2017). Assessing the resiliency of surface water and groundwater systems under groundwater pumping. *Hydrology and Earth System Sciences Discussions*, 1–47.

Singer, A. (1970). Weathering products of basalt in the galilee. i. rock-soil interface weathering. *Israel Journal of Chemistry*, *8*(3), 459-468. Retrieved from https://onlinelibrary.wiley.com/doi/abs/10.1002/ijch.197000052 doi: https://doi.org/10.1002/ijch.197000052

Tørå, G., Hansen, A., & Oeren, P.-E. (2010, 09). Dynamic network modeling of resistivity index in a steady-state procedure. *Proceedings - SPE Annual Technical Conference and Exhibition*, *6*. doi: 10.2118/135367-MS

van Buurt, G. (2009). A short natural history of curaçao. , *1*, 229–256.

WAITT. (2016). *Marine scientific assessment: the state of curaçao's reef communities.* WAITT Institute.

Westermann, J. (1949). Overzicht van de geologische en mijnbouwkundige kennis der nederlandse antillen.

WMO. (2021, Sep). *El niño/la niña southern oscillation (enso).* Retrieved from https://public.wmo.int/en/our-mandate/climate/el-niñola-niña-update

Appendix

I Geological map (Beets, 1977)

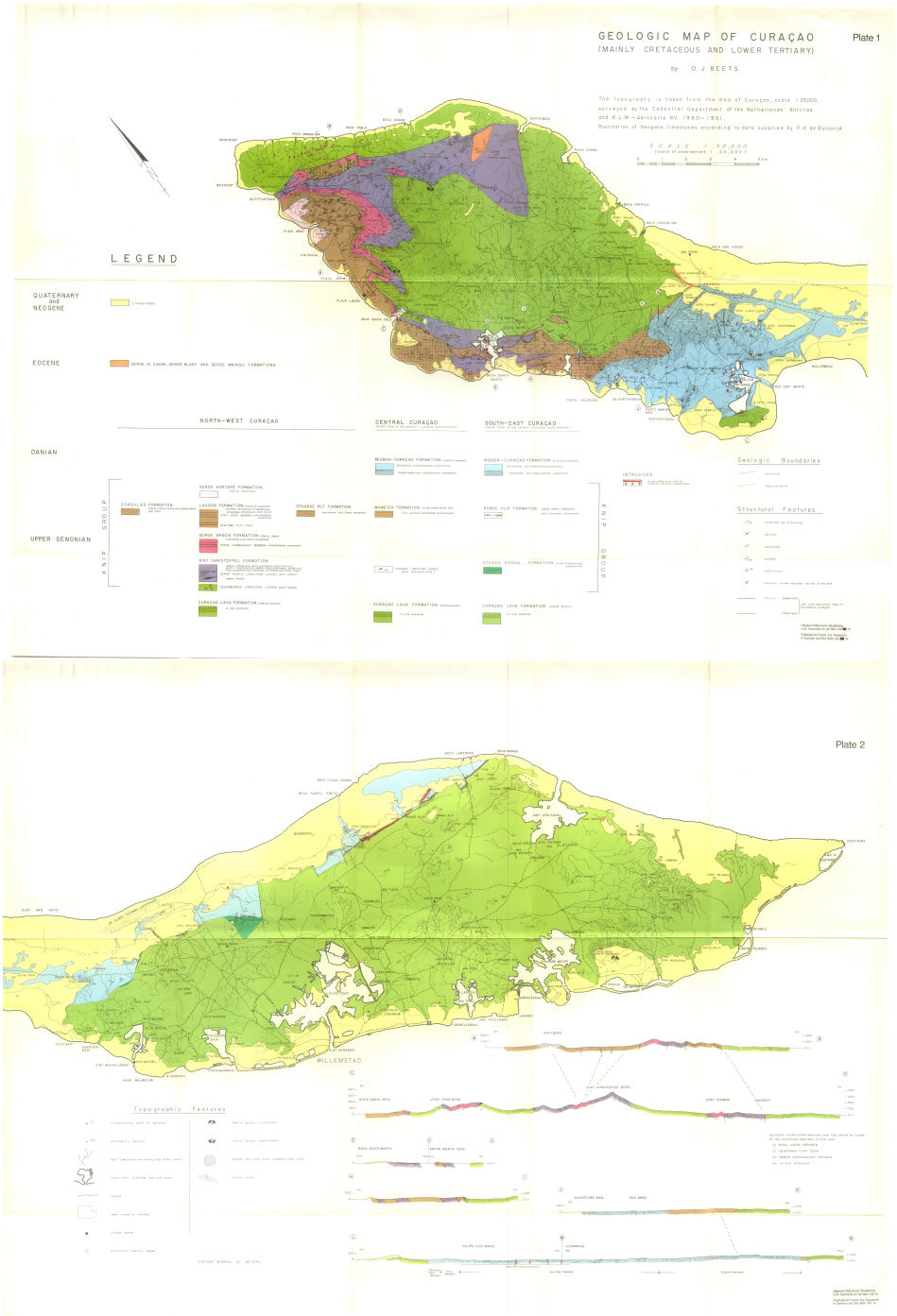

Figure 1: Geological maps of east and western part of Curaçao.(Beets, 1977)

II Geological Borehole Descriptions

Figure 2: Geological borehole descriptions (Abtmaier, 1978)

Depth [m]	**4N112** *Midden Formation*
4	Limestone
7	Silt & Limestone
13	Limestone
18	Silt, Clay & Limestone

Depth [m]	**5N275** *Lava formation*	**5N276** *Lava formation*
2	clay	clay & weathered basalt
4	clay silt	
6	basalt & coarse sand	highly fractured basalt
10	highly fractured basalt & clay	fractured basalt
12	fractured basalt	
26	slightly fractured basalt	slightly fractured basalt

III Initial Inversion model Errors

para, cen,

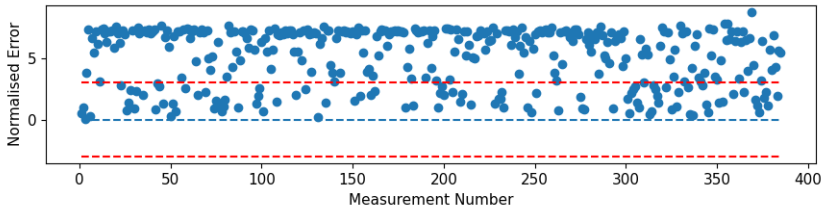

Figure 3: Initial inversion errors in the DD at Parallel weg

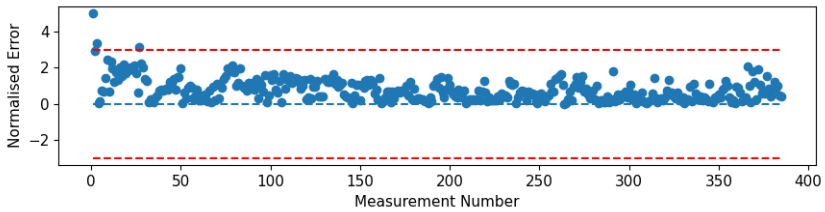

Figure 4: Initial inversion errors in the DD at Centrum Supermarket PSB

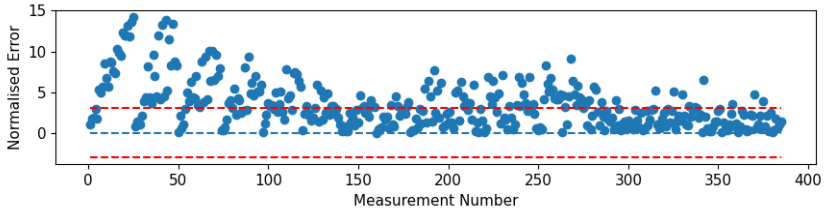

Figure 5: Initial inversion errors in the DD at Piscadera Bay Inlet

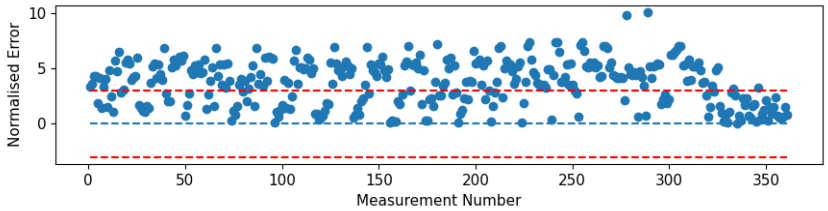

Figure 6: Initial inversion errors in the DD at Rooi Rincon

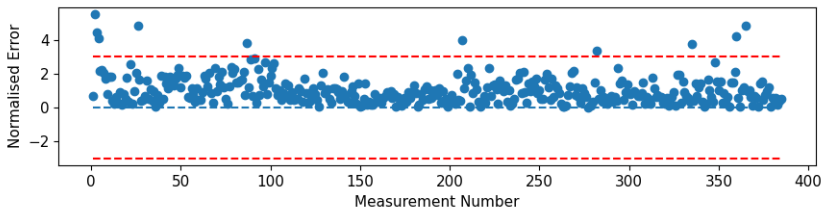

Figure 7: Initial inversion errors in the DD at Race Track

IV Groundwater Measurements and Monitoring

Table 1: start and ending date of the data to compute the slope along with the observed change in GWL (cm) and the resulting slope (cm/d)

	GW072	Mark	GW077	5Z19A	5Z19B	5Z19B Pumped	GW006	GW014
start date	26/11/2021	07/12/2021	30/11/2021	01/12/2021	01/12/2021	08/12/2021	02/12/2021	30/11/2021
end date	03/01/2022	19/12/2021	02/12/2021	10/12/2021	04/12/2021	13/12/2021	05/12/2021	09/12/2021
/Delta gwl (cm)	81.3	26	19.1	34.4	19.4	4.4	8.5	33.7
slope (cm/d)	2.1	2.2	13.1	3.7	6.2	0.9	2.5	4.1

V Hato Spring

Table 2: The monthly measured discharge and EC of Hato spring from October 1977 till February 1978 (Abtmaier, 1978)

date	Oct/76	Nov/76	Dec/76	Jan/77	Feb/77	Mar/77	Apr/77	May/77	Jun/77	Jul/77	Aug/77	Sep/77	Oct/77	Nov/77	Dec/77	Jan/78	Feb/78
Q	0.74		0.83		0.7		0.79		1.05	0.98	1.02		0.86	0.9	0.77	0.86	0.68
EC	810		1320		1280		1150			1260	1400		1350	1400	1400	1400	1600

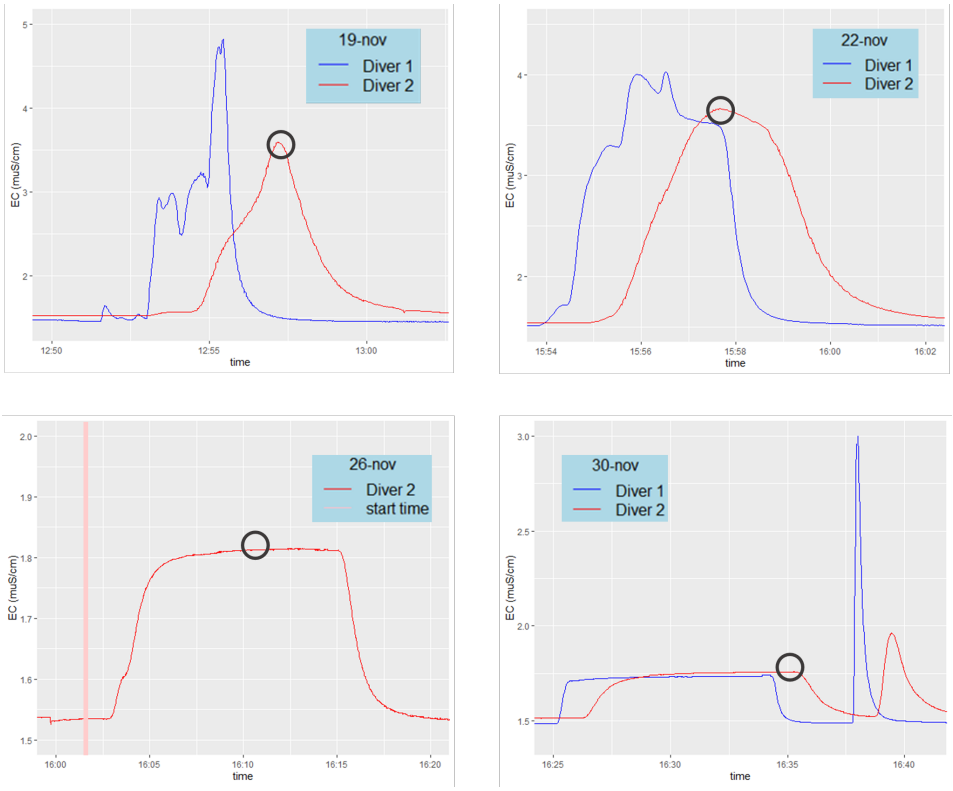

Figure 8: The plots of the salt dillution experiments. On 26 November there was only one diver available. This complicated the velocity calculation. The black circles in the graph depict the ECss used in the discharge calculations.